CrossMark

ORIGINAL PAPER

Phase diagrams, thermodynamic properties and sound velocities derived from a multiple Einstein method using vibrational densities of states: an application to MgO–SiO$_2$

Michael H. G. Jacobs[1] · Rainer Schmid-Fetzer[1] · Arie P. van den Berg[2]

Abstract In a previous paper, we showed a technique that simplifies Kieffer's lattice vibrational method by representing the vibrational density of states with multiple Einstein frequencies. Here, we show that this technique can be applied to construct a thermodynamic database that accurately represents thermodynamic properties and phase diagrams for substances in the system MgO–SiO$_2$. We extended our technique to derive shear moduli of the relevant phases in this system in pressure–temperature space. For the construction of the database, we used recently measured calorimetric and volumetric data. We show that incorporating vibrational densities of states predicted from ab initio methods into our models enables discrimination between different experimental data sets for heat capacity. We show a general technique to optimize the number of Einstein frequencies in the VDoS, such that thermodynamic properties are affected insignificantly. This technique allows constructing clones of databases from which we demonstrate that the VDoS has a significant effect on heat capacity and entropy, and an insignificant effect on volume properties.

✉ Michael H. G. Jacobs
    Michael.jacobs@TU-Clausthal.de

[1] Institute of Metallurgy, Clausthal University of Technology, Robert Koch Str. 42, 38678 Clausthal-Zellerfeld, Germany

[2] Department of Theoretical Geophysics, Utrecht University, Budapestlaan 4, 3584 CD Utrecht, The Netherlands

Introduction

The goal of our work is to establish a thermodynamic database for planetary mantle materials. Such databases are a requirement for constructing self-consistent models of planetary interiors that can be applied in the interpretation of geophysical observations. In Jacobs et al. (2013), we recently developed a semi-empirical method based on the vibrational density of states (VDoS) of a material that can be used advantageously to represent its thermodynamic properties in a simple and accurate manner. The method is related to Kieffer's (1979) lattice vibrational method and enables incorporation of a realistic representation of the VDoS. An advantage of our method is that it does not require details of the crystallographic structure to establish the number of vibrational normal modes in specific frequency ranges, thereby reducing the complexity of the method, and making it a useful tool for thermodynamic database development. Compared to methods that represent the properties in the Gibbs energy expression with function parameterizations or the Mie–Grüneisen–Debye (MGD) method, our method enables constraining a thermodynamic analysis with results derived from modern ab initio methods, in particular the VDoS, static properties and Grüneisen parameters. That is extremely useful when adding substances to a database for which thermodynamic data are scant, or not even present, such as for materials in the deep mantle of heavy exoplanets as for instance predicted by Umemoto and Wentzcovitch (2011). Because our method is constrained by the VDoS, the thermodynamic description of a substance is better constrained by low-temperature heat capacity data, derived from PPMS or adiabatic calorimetry, relative to function parameterization methods. As we shall demonstrate for wadsleyite, ringwoodite and akimotoite, low-temperature heat capacity data are important

for constraining high-temperature heat capacity. Relative to the MGD method, our method has the advantage that both low- and high-temperature heat capacity data are more accurately represented.

Although we applied our method in Jacobs et al. (2013) to a number of substances, we did not show its applicability in a full thermodynamic analysis of a system involving multi-phase equilibria. To be successful, our method should represent not only thermodynamic properties of a specific substance to within experimental uncertainty, but also complex phase equilibria and experimental enthalpy differences between that substance and other substances. In addition to our method presented in Jacobs et al. (2013), we implemented a method developed by Stixrude and Lithgow-Bertelloni (2005) to calculate mechanical properties, such as the shear modulus. That enables us predicting longitudinal and transverse sound velocities at conditions difficult to access by experimentation and to compare our results with seismic experiments.

As vehicle to test our method in a full thermodynamic analysis of experimental data, we selected the system MgO–SiO$_2$, which forms a cornerstone system of the larger system CaO–FeO–MgO–Al$_2$O$_3$–SiO$_2$ (CFMAS), a canonical system for approximating material compositions of planetary mantles. Addressing the smaller binary system is a necessary first step in the development of a thermodynamic database for ceramic and planetary mantle materials. We selected this system because of the wealth of experimental data that are available for substances appearing in it, making it eligible for testing the accuracy of our method. Moreover, for all polymorphs, a VDoS is available predicted by ab initio techniques. The system MgO–SiO$_2$ has been the subject of several thermodynamic analyses, such as by means of parameterization techniques by Saxena (1996), Holland and Powell (1998) and Fabrichnaya et al. (2004), and by semi-empirical methods such as the MGD method by Stixrude and Bertelloni (Stixrude and Lithgow-Bertelloni 2005, 2011) and Kieffer's (1979) method by Jacobs and de Jong (2007). Since the time these works were published, new experimental data have become available for heat capacity and volume for many polymorphic substances in the system MgO–SiO$_2$, such as for forsterite, wadsleyite, ringwoodite, perovskite, akimotoite, and stishovite, which put tighter constraints on a thermodynamic analysis. In our analysis, we pay special attention to representing data at 1 bar pressure as accurate as possible because these data do not suffer from pressure scale effects. In our analysis, we used a single pressure scale to represent thermodynamic data for all substances in pressure–volume–temperature (P–V–T) space. That enabled us to point to inconsistencies in experimental data especially when more than one pressure scale has been used for the same substance, such as for stishovite. Moreover, this gives

us the opportunity to extend our small database to multi-component systems in a transparent manner when new insights into pressure scales become available. For this purpose, we have chosen the pressure scale of Dorogokupets and Oganov (2007), which is consistent for a series of elements, MgO and ruby.

To represent accurately all features in the VDoS predicted by ab initio methods, we generally used sixty Einstein frequencies for all substances. However, for representing thermodynamic properties, this is a generously large number. Therefore, we investigated the effect of reducing the number of frequencies on thermodynamic properties, keeping all other model parameters, such as static lattice properties and Grüneisen parameters unchanged. We show a systematic process to optimize the number of frequencies in the VDoS of each substance, requiring that thermodynamic properties and phase diagrams are changed insignificantly.

Theoretical background

Our models are based on a semi-empirical expression for the Helmholtz energy, which we separate into static lattice, vibrational, electronic and magnetic effects. Because the substances in the system MgO–SiO$_2$ are solid insulator materials, we omit the electronic and magnetic terms and write the Helmholtz free energy of a substance as an analytical function of temperature, T, and volume, V:

$$A(T, V) = U^{\text{ref}} + U^{\text{static}}(V) + A^{\text{vib}}(T, V) \qquad (1)$$

The first term in Eq. (1) represents the reference energy at zero Kelvin and zero pressure. For MgO, Mg$_2$SiO$_4$ (forsterite) and MgSiO$_3$ (orthoenstatite), we adjusted values for this property such that their heats of formation from the elements at 298.15 K and 1 bar are represented. For the other polymorphs in the system MgO–SiO$_2$, for which no such data are available, we used enthalpy difference measurements and locations of phase boundaries.

Static lattice and vibrational properties

The static lattice contribution to the Helmholtz energy in the second term of Eq. (1) is based on an equation of state, for which Jacobs et al. (2013) selected that of Vinet et al. (1989). However, many works describing the construction of a thermodynamic database, such as Saxena (1996), Fabrichnaya et al. (2004) and Stixrude and Lithgow-Bertelloni (2005, 2011) employ the Birch–Murnaghan (BM) equation of state. Jacobs et al. (2007) showed that differences between results obtained with these two equations of state are insignificant in large ranges of temperature and pressure for substances in MgO–SiO$_2$. In additional, parallel

Table 1 Relation between coefficients in the expressions (2)–(6) and static properties to fourth order in strain in the expression for Helmholtz free energy

EoS order	v	a_v	b_v
2	2	$9K_0^{st}$	G_0^{st}
3	3	$27K_0^{st}\left(K_0^{'st}-4\right)$	$3K_0^{st}\left(G_0^{'st}-1\right)-7G_0^{st}$
4	4	$81K_0^{st}\left[K_0^{st}K_0^{''st}+K_0^{'st}\left(K_0^{'st}-7\right)+\frac{143}{9}\right]$	$9\left(K_0^{st}\right)^2 G_0^{''st}+3K_0^{st}\left(G_0^{'st}-1\right)\left(3K_0^{'st}-16\right)+63G_0^{st}$

The coefficients apply at zero Kelvin and zero pressure

analyses using Vinet's equation of state, we find the same conclusions as we present here using the BM equation of state. In the analyses shown here, we have omitted liquid, for which Ghiorso (2004) showed that Vinet's equation of state leads to better results than the BM equation of state. To facilitate comparing our derived static properties with parameters derived in previous works above, we adopt the BM equation of state. Moreover, Stixrude and Lithgow-Bertelloni (2005, 2011) presented an elegant framework based on finite strain theory, which enables expressing the shear modulus of a substance, which justifies using the BM equation of state for pressure. Because shear modulus is related to the equation of state, we cast these expressions into more practicable ones using a formulation by Anderson (1998). The coefficients in these equations are related to bulk modulus, shear modulus and their pressure derivatives. These relations are given in Table 1. For a Nth order equation of state:

Helmholtz energy:
$$A^{\text{static}}(f) = V_0^{\text{st}} \sum_{v=2}^{N}\left(a_v \frac{f^v}{v!}\right) \tag{2}$$

Pressure:
$$P^{\text{static}}(f) = \frac{1}{3}(1+2f)^{5/2} \sum_{v=2}^{N}\left(a_v \frac{f^{v-1}}{(v-1)!}\right) \tag{3}$$

Bulk modulus:
$$K^{\text{static}}(f) = \frac{1}{9}(1+2f)^{5/2}$$
$$\times\left\{5\sum_{v=2}^{N}\left(a_v \frac{f^{v-1}}{(v-1)!}\right)+(1+2f)\sum_{v=2}^{N}\left(a_v \frac{f^{v-2}}{(v-2)!}\right)\right\} \tag{4}$$

Shear modulus: $G_{\text{shear}}^{\text{static}}$
$$= (1+2f)^{5/2} \sum_{v=2}^{N}\left\{\left[b_v+\left(2b_v+\frac{a_v}{3(v-1)}\right)f\right]\frac{f^{v-2}}{(v-2)!}\right\} \tag{5}$$

Strain:
$$f = \frac{1}{2}\left[\left(\frac{V}{V_0^{st}}\right)^{-2/3}-1\right] \tag{6}$$

For anisotropic substances, we treat the shear modulus as that of an isotropic polycrystalline aggregate and use Voigt–Reuss–Hill averages to obtain values for the shear modulus properties in Table 1. For all substances in the system MgO–SiO₂, we use a third-order equation of state, with the exception of orthoenstatite, for which we used a fourth-order equation of state.

Equations (2)–(6) illustrate that the static pressure and static Helmholtz free energy have zero values at volume V_0^{st} and that bulk modulus is K_0^{st} and shear modulus is G_0^{st}. These are the equilibrium properties of a substance in which vibrational motions are absent and in that case, the external pressure equals the static pressure. However, for a real substance, vibrational contributions must be included in the Helmholtz free energy, even at zero Kelvin, represented by the third term in Eq. (1). We use expressions given by Jacobs et al. (2013), in which intrinsic anharmonicity is incorporated using the perturbation method presented by Oganov and Dorogokupets (2004). The vibrational contribution to Helmholtz free energy is written in terms of N_E Einstein temperatures, $\theta_j^E = h v_j^E / k$, associated with N_E Einstein frequencies v_j^E, and their fractions related to the VDoS, f_j. Because a misprint occurred in our previous work, we reformulate the expression for the Helmholtz energy below. Using symbol R for the gas constant and n for the number of atoms per molecular formula, the expression is:

$$A^{\text{vib}}(T,V)$$
$$= 3nRT \sum_{j=1}^{N_E} f_j \left[\frac{\theta_j^E}{2T}+\ln\left(1-\exp\left(-\frac{\theta_j^E}{T}\right)\right)\right]$$
$$+ A_{\text{anh}}^{\text{vib}}(T,V) \tag{7}$$

$$A_{\text{anh}}^{\text{vib}}(T,V) = 3nRT^2 \sum_{j=1}^{N_E} \frac{a_j^{\text{anh}}}{6} f_j$$
$$\times\left[\frac{1}{4}\left(\frac{\theta_j^E}{T}\right)^2+\frac{3\left(\theta_j^E/T\right)^2 \exp\left(\theta_j^E/T\right)}{\left(\exp\left(\theta_j^E/T\right)-1\right)^2}\right] \tag{8}$$

The anharmonicity parameters a_j^{anh} can be made volume dependent, which we use only for MgO. In our previous work, a scheme is given to determine the Einstein frequencies or temperatures and their fractions from the VDoS. The vibrational contribution to shear modulus is related to the vibrational contribution to energy. We follow Stixrude and Lithgow-Bertelloni (2005) and formulate it as:

$$G_{\text{shear}}^{\text{vib}}(T,V) = -\frac{3nR}{V} \sum_{j=1}^{N_E} n_{s,j} f_j \theta_j^E \left(\frac{1}{2} + \frac{1}{\exp\left(\theta_j^E \big/ T\right) - 1} \right) \quad (9)$$

In Eq. (9), $n_{s,j}$ represents the shear derivative of the Gruneisen parameter of the jth Einstein temperature. To keep the formalism transparent and consistent with that of Stixrude and Lithgow-Bertelloni (2011), we follow their expressions relating vibrational Einstein temperatures and Eulerian finite strain. By taking this step, we deviate from our own expressions in Jacobs et al. (2013) relating frequencies and Grüneisen parameters with volume. For isotropic substances, Einstein temperatures are given by:

$$\left(\theta_j^E\right)^2 = \left(\theta_{j,0}^E\right)^2 \left(1 + a_{ii,j}^{(1)} \phi + \frac{1}{2} a_{iikk,j}^{(2)} \phi^2 + \cdots \right) \quad (10)$$

In Eq. (10), the isotropic strain, φ, is given by:

$$\phi = \frac{1}{2} \left[\left(\frac{V}{V_0} \right)^{-2/3} - 1 \right] \quad (11)$$

Values for the strain, φ, deviate slightly from the strain, f, given in Eq. (6), because the volume V_0 of the substance at zero Kelvin and zero pressure is slightly larger that the volume of the static lattice, V_0^{st}.

From the definition of the Grüneisen parameter, we find:

$$\gamma_j = -\left(\frac{\partial \ln \theta_j^E}{\partial \ln V} \right)_T = \frac{1}{6} \left(\frac{\theta_{j,0}^E}{\theta_j^E} \right)^2 (2\phi + 1)\left(a_{ii,j}^{(1)} + a_{iikk,j}^{(2)} \phi \right) \quad (12)$$

$$V\left(\frac{\partial \gamma_j}{\partial V} \right)_T = \gamma_j q_j = \frac{1}{9} \left(18\gamma_j^2 - 6\gamma_j - \frac{1}{2} \left(\frac{\theta_{j,0}^E}{\theta_j^E} \right)^2 (2\phi + 1)^2 a_{iikk,j}^{(2)} \right) \quad (13)$$

Grüneisen parameters appear in the expressions of vibrational contribution to pressure, its temperature derivative at constant volume and bulk modulus. The property given by Eq. (13) appears only in bulk modulus, Eq. (18) in Jacobs et al. (2013). The shear strain derivatives $n_{s,j}$ in Eq. (9) for the shear modulus contribution are given by:

$$n_{s,j} = -\gamma_j + \left(\frac{\theta_j^E}{\theta_{j,0}^E} \right)^2 (2\phi + 1)^2 (\gamma_{j,0} + n_{s,j,0}) \quad (14)$$

Finally, the coefficients $a_{ii,j}^{(1)}$ and $a_{iikk,j}^{(2)}$ are related to the Grüneisen parameters and mode-q parameters as:

$$a_{ii,j}^{(1)} = 6\gamma_{j,0} \quad (15)$$

$$a_{iikk,j}^{(2)} = -12\gamma_{j,0} + 36\gamma_{j,0}^2 - 18\gamma_{j,0} q_{j,0} \quad (16)$$

The N_E input model parameters for the vibrational part of each of the properties $\gamma_{j,0}$, $q_{j,0}$, $n_{s,j,0}$, and $\theta_{j,0}^E$ refer to zero Kelvin, zero pressure. It appears that most polymorphs in the system MgO–SiO$_2$ can be treated as monodisperse in Grüneisen parameters without significant loss in accuracy for representing experimental thermodynamic properties. That reduces the number of these model parameters to γ_0, q_0, $n_{s,0}$, $\theta_{j,0}^E$. With the expressions above for frequency and Grüneisen parameter, the same expressions for vibrational contributions to thermodynamic properties apply as given by Jacobs et al. (2013). The advantage of the formalism is that shear modulus defined by Eqs. (5), (9) and (14) can be treated independently from the thermodynamic analysis. Therefore, shear modulus descriptions can be post-processed after a thermodynamic analysis has been carried out. Disadvantage is that shear modulus data do not put tighter constraints on a thermodynamic analysis of experimental data.

Landau contribution

We have applied Landau and Lifshitz (1980) formalism for describing the transition from the tetragonal rutile form of SiO$_2$, stishovite to the orthorhombic CaCl$_2$ form of SiO$_2$, which we denote, following Oganov et al. (2005), as SiO$_2$(I). The formalism is a macroscopical one, and it is based on the Gibbs free energy instead of the Helmholtz energy. According to Carpenter (1992), Hemley et al. (2000), Andrault et al. (2003) and Oganov et al. (2005), the transition is second order in nature. The Gibbs energy is given by:

$$G^{\text{total}}(P,T) = G(P,T) + G^{\text{Landau}}(P,T) \quad (17)$$

Equation (17) applies to the Gibbs energy of both stishovite and SiO$_2$(I). The first term on the right-hand side of Eq. (17) denotes the Gibbs free energy calculated with the Helmholtz free energy, Eq. (1), and applies to stishovite, whereas the second term on the right-hand side applies to SiO$_2$(I). The Landau contribution to Gibbs energy for the second-order transition is expressed by the order parameter Q, which is zero for the stishovite phase and between zero and one for the SiO$_2$(I) phase. Following Putnis (1992), we write it as:

$$G^{\text{Landau}} = \frac{1}{2} a_L [T - T_c(P)] Q^2 + \frac{1}{4} B Q^4 \quad (18)$$

In Eq. (18), $T_c(P)$ represents the critical temperatures along the phase boundary between stishovite and $SiO_2(I)$, which we express in terms of the inverse of its Clapeyron slope, h, as:

$$T_c(P) = T_c(P = 0) + h \times P \tag{19}$$

From the equilibrium condition $(\partial G^{Landau}/\partial Q)_{P,T} = 0$ and by using the definition that $Q = 1$ at $T = 0$, we obtain the expression for Gibbs energy and order parameter as:

$$G^{Landau} = \frac{1}{2}a_L\left\{[T - T_c(P)]Q^2 + \frac{1}{2}T_c(P)Q^4\right\} \tag{20}$$

$$Q^2 = \frac{T_c(P) - T}{T_c(P)}, \quad B = a_L T_c(P) \tag{21}$$

In the thermodynamic analysis of volume data for $SiO_2(I)$, we fix the location of the phase boundary and its inverse Clapeyron slope, h, and fitted the free parameter a_L. Other thermodynamic properties derived from Eqs. (17) and (18) are given in the Appendix.

Results

The description of the system MgO–SiO$_2$ requires determination of phase equilibria in the two sub systems Mg$_2$SiO$_4$ and MgSiO$_3$, which are linked together by the phases wadsleyite, ringwoodite, akimotoite, perovskite and stishovite. We used the same data set as Jacobs and de Jong (2007) extended with new data sets that have become available since 2007. Compared to their analysis, we extended the thermodynamic description with the phase low-clinoenstatite, and two high-pressure polymorphs of SiO$_2$. Figures 1 and 2 show the phase diagrams of Mg$_2$SiO$_4$ and MgSiO$_3$ resulting from our analysis. Model parameters for all fourteen phases are given in Tables 2, 3 and "online resource Table 1" and were derived using experimental and ab initio data given in "online resource Table 2" and Table 4. We used vibrational densities of states (VDoS) derived by ab initio techniques for all polymorphs, such as illustrated in Fig. 3 for wadsleyite and ringwoodite. We employed the same method as in Jacobs et al. (2013) to partition the VDoS for these polymorphs in 60 Einstein continua, illustrated as the coloured boxes underneath the VDoS curve, and subsequently we placed one Einstein monochromatic frequency in the middle of each box. That enabled us to use the same expressions for thermodynamic properties as given in our previous work.

Our method is semi-empirical. The model parameters were obtained by fitting them to available data sets, such that the majority of data are represented as accurate as possible. In the analysis of these data, we shifted frequencies in the VDoS of a polymorph, all with the same amount by less
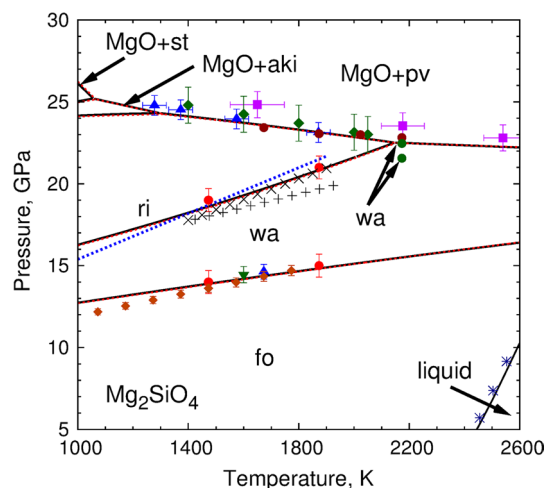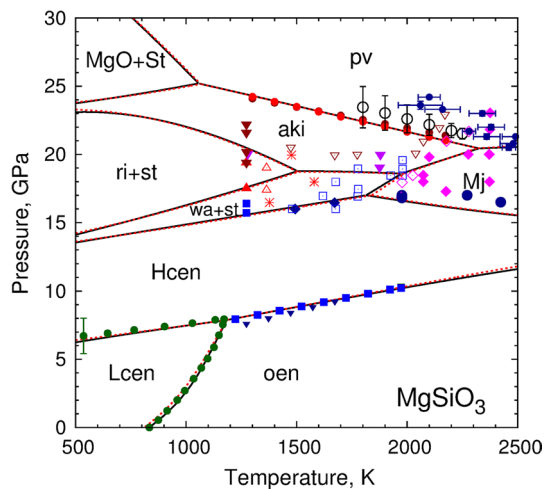

Fig. 1 Phase diagram of Mg$_2$SiO$_4$ calculated with a database in which the VDoS of each polymorph is represented by 60 Einstein frequencies, indicated by *solid black* curves, is insignificantly different from that calculated by a database in which each VDoS is represented by a single Einstein frequency, indicated by the *dashed red curves*. Experimental data are from: *post-spinel* Ito and Takahashi (1989, *triangle*), Shim et al. (2001, *diamond*), Chopelas et al. (1994, *square*), Fei et al. (2004, *circle*, including wa); *wadsleyite–ringwoodite* Inoue et al. (2006, *plus*), Gasparik (2003, *cross*), Suzuki et al. (2000, *dashed line*), Katsura and Ito (1989, *circle*); *forsterite–wadsleyite* Fei and Bertka (1999, *triangle*), Morishima et al. (1994, *diamond*), Boehler and Chopelas (1991, *inverse triangle*), Katsura and Ito (1989, *circle*). The phase boundary between liquid and forsterite has been drawn tentatively using experimental data of Ohtani and Kumazawa (1981)

than 5 cm^{-1}, to find the best representation of heat capacity data below room temperature. Fractions of the VDoS, associated with the Einstein temperatures, were not optimized, but directly determined from the VDoS. In "online resource Table 2", Tables 4 and 6, a comparison is given between experimental and our calculated thermodynamic properties.

Expressions for shear modulus were established by fitting shear modulus data or longitudinal and shear sound velocities after the thermodynamic description of the system was completed.

Details of the optimization

We used a least-squares nonlinear optimization technique to establish values for model parameters. Values for experimental data are determined by random and systematic uncertainties. To reduce the effect of systematic uncertainties at pressure, we used a single pressure scale for all substances. Systematic uncertainties due to the use of different experimental devices are also present in 1 bar experimental data, such as in thermal expansivity and volume of forsterite, shown in, for example, Figure 10 of Jacobs et al. (2013). For that reason, we performed a multitude of thermodynamic analyses to elucidate which data sets are

Fig. 2 Phase diagram of MgSiO₃ calculated with a database in which the VDoS of each polymorph is represented by 60 Einstein frequencies, indicated by *solid black curves*, is insignificantly different from that calculated by a database in which each VDoS is represented by a single Einstein frequency, indicated by the *dashed red curves*. Experimental data are from: *aki = pv* combination of Ono et al. (2001) and Hirose et al. (2001), *dark solid circles* by using the MgO scale of Speziale et al. (2001), *red solid circles* by using the MgO pressure scale of Dorogokupets and Oganov (2007), Chudinovskikh and Boehler (2004, *open circle*, *pv solid circles* with *error bars*); *aki* Kanzaki (1987, inverse *solid triangles* at 1273 K), Sawamoto (1987, *inverse open triangle*), Ito and Navrotsky (1985, *solid inverse triangle*); *ri + st* Kanzaki (1987, *solid triangle*, 1273 K), Sawamoto (1987, *asterik*), Ito and Navrotsky (1985, *open triangle*); *mj* Presnall and Gasparik (1990, *solid circle*), Sawamoto (1987, *open diamond*: mj + pv and mj + aki, *solid diamond*: mj); *wa + st* Kanzaki (1987, *solid square* at 1273 K), Sawamoto (1987, *open square*); *hcen = wa + st* Presnall and Gasparik (1990, *solid diamond*); *oen = cen* Pacalo and Gasparik (1990, *solid square*), Kanzaki (1991, *inverse triangle*); *Lcen = oen* Angel and Hugh-Jones (1994, *solid circle*); *Lcen = Hcen* Angel and Hugh-Jones (1994, *solid circle*)

consistent with each other. In the text of "online resource", we detail results of analyses of each substance separately.

We performed analyses of data in two sequences. In the first one, we focussed on thermophysical properties of all substances separately. In this sequence, heat capacity data below room temperature form key experimental information to constrain vibrational frequencies at zero temperature and zero pressure. At low temperatures, the difference between isobaric and isochoric heat capacity is insignificantly small, such that the analysis is not affected by parameters other than frequencies at zero temperature and zero pressure, such as depicted in Fig. 3 for wadsleyite and ringwoodite. Generally, we performed optimizations in which all data sets were assigned equal weight. We noticed that dispersion in Grüneisen parameters has no significant effect on the representation of experimental data, with the exception of forsterite and majorite. Grüneisen and mode-*q* parameters were in all cases constrained well by experimental thermal expansivity and bulk modulus data

at 1 bar pressure and by ab initio predictions in pressure–temperature space, resulting in accurate representations of volume data, such as demonstrated in Fig. 4 for ringwoodite, perovskite and stishovite. In this sequence of optimizations, we applied the quasi-harmonic approximation to all substances except for two substances. One exception is forsterite, for which mode anharmonicity parameters were measured by Gillet et al. (1991). The other exception is MgO in which volume-dependent anharmonicity must be incorporated. Because values of model parameter for all substances are not very different, simple optimization techniques, such as a combination of steepest descent and alternate minimization of the sum of squares, produced rapid convergence and robust results, independent of starting values. This sequence results in a number of findings, the most important of which are given here. Generally, the VDoS of each substance is of such quality that low-temperature heat capacity is accurately represented. That in turn puts better constraints on high-temperature heat capacity, such as demonstrated for wadsleyite and ringwoodite for which the most recent high-temperature heat capacity data of Jahn et al. (2013) and Kojitani et al. (2012) are preferred over older DSC data. By constraining dispersion in Grüneisen parameters of forsterite with spectroscopic data, our analysis prefers the *V–T* data of Kajiyoshi (1986), consistent with thermal expansivity predicted by Li et al. (2007). By using data for MgO resulting from primary pressure scales, we arrived at a description consistent with ab initio predictions of Wu et al. (2008). By applying a single pressure scale to SiO₂, we found that the effect of a second-order phase transition between the stishovite and CaCl₂ forms on volume is smaller than expected by Andrault et al. (2003).

In the second sequence of optimizations, we included phase diagram data depicted in Figs. 1 and 2. We refrained from a global optimization because phase boundaries were not established with equal robustness experimentally. Instead, we focussed first on phase boundaries which are robust or which could be constrained more robustly by using enthalpy difference data. These boundaries were subsequently used to constrain those which are less certain. For that reason, we started with phase boundaries between forsterite, wadsleyite and ringwoodite because they can be tightly constrained by using enthalpy differences, measured at two temperatures by Akaogi et al. (1989, 2007). Heat capacity data of wadsleyite and ringwoodite measured by the PPMS technique alone are clearly not sufficiently accurate enough to favour a specific phase boundary between these forms. Because the effect of changing parameters affecting volume properties on these phase boundaries is too small, we achieved a description to within experimental uncertainty of all properties by changing anharmonicity parameters of wadsleyite and forsterite, staying within the uncertainties of heat capacities. In this part of the

Table 2 Model parameters for the static lattice of polymorphs for which the VDoS is described with 60 Einstein frequencies

	U^{ref}/kJ/mol	V_0	V_0^{st}	K_0^{st}/GPa	$K_0'^{st}$	G_0/GPa	$G_0'^{st}$
Fo	−2251.75 (100)	43.513 (12)	43.018 (12)	136.26 (50)	4.43 (11)	87.41 (40)	1.50 (7)
Fo(*)	−2251.75 (100)	43.492 (12)	43.069 (12)	135.04 (50)	4.43 (11)	87.41 (40)	1.50 (7)
Wa	−2224.30 (155)	40.388 (12)	39.957 (12)	178.19 (70)	4.30 (16)	119.85 (80)	1.52 (12)
Ri	−2213.50 (155)	39.404 (12)	39.005 (12)	191.77 (88)	4.21 (17)	128.37 (84)	1.41 (17)
Pc	−621.09 (30)	11.203 (5)	11.074 (5)	171.37 (50)	4.19 (11)	139.80 (50)	2.27 (15)
St &	−909.08 (100)	13.999 (6)	13.873 (6)	319.32 (80)	4.08 (6)	237 (4)	1.92 (10)
St-I	$a_L = 0.0126$ JK^{-1} mol^{-1}, $h = 1.593 \times 10^{-7}$ K/Pa, T_c ($P = 0$) = −7071.35 K, Eqs. (19, 20)						
Si-II	−894.77 (100)	13.773 (6)	13.659 (6)	324.43 (80)	4.23 (6)	247 (4)	1.87 (10)
Pv	−1504.05 (200)	24.386 (9)	24.145 (9)	256.28 (135)	4.00 (7)	182.5 (15)	1.71 (4)
Pv(*)	−1505.44 (200)	24.449 (9)	24.209 (9)	256.21 (135)	3.98 (7)	182.5 (15)	1.71 (4)
Ppv	−1476.35 (247)	24.205 (9)	23.930 (9)	243.85 (90)	4.16 (6)	148.2 (10)	2.10 (20)
Ppv(*)	−1499.34 (247)	24.641 (9)	24.353 (9)	230.04 (90)	4.26 (6)	148.2 (10)	2.10 (20)
Aki	−1553.96 (200)	26.292 (9)	26.024 (9)	224.11 (200)	5.57 (77)	142.1 (45)	1.58 (13)
Mj	−1565.53 (200)	28.334 (38)	28.065 (38)	171.66 (100)	4.16 (30)	92.32 (32)	1.54 (14)
Hcen	−1597.73 (150)	30.277 (8)	29.860 (8)	127.28 (70)	6.01 (18)	96.47 (42)	1.73 (6)
Lcen	−1602.75 (130)	31.179 (10)	30.795 (10)	120.44 (150)	6.23 (100)	84.31 (60)	1.50 (10)
					−		−0.20 (2)
Oen	−1601.92 (100)	31.223 (6)	30.836 (6)	118.83 (70)	7.46 (40)	83.20 (60)	1.50 (10)
					−0.44 (17)		−0.21 (2)

Orthoenstatite and Low-pressure clinoenstatite are described with a fourth order-Birch–Murnaghan EoS. The fourth-order coefficients K_0^{st} and G_0^{st} are written on the line below the substance. Fo(*) denotes a description for forsterite in which dispersion in Grüneisen parameter is incorporated. St-I denotes the CaCl$_2$ form of SiO$_2$ and is described with the same VDoS as stishovite. Pv(*) and Ppv(*) are results from an alternative analysis in which our description for MgO (pc) is used as a pressure scale. Volumes are given in cm^3/mol

optimization, we made use of the characteristic that intrinsic anharmonicity insignificantly affects volume properties as long as it is volume independent, which applies to all substances except for MgO. Mainly due to the enthalpy difference data, our description prefers the boundaries measured by Katsura and Ito (1989). The resulting description for ringwoodite is used to constrain the post-spinel phase boundary.

We represented data for the post-spinel phase boundary and that between akimotoite and perovskite by optimizing anharmonicity parameters of perovskite and akimotoite. That was achieved by accepting that the anharmonicity parameter of perovskite is—(0.25 ± 0.25 × 10^{-5} K^{-1} (GilletP et al. 2000) and that of akimotoite is—(0.9 ± 0.7) × 10^{-5} K^{-1} (Reynard and Rubie 1996b). Additionally, we used as constraint the location of the phase junction at which MgO, perovskite, akimotoite, and ringwoodite are at equilibrium in the Mg$_2$SiO$_4$ phase diagram, predicted by ab initio by Yu et al. (2011). Because the description for MgO is robust, we did not change its parameters resulting from the first sequence, except for its reference energy. At this stage, an accurate representation of experimental data in the Mg$_2$SiO$_4$ phase diagram was completed and the results were used to constrain the remaining less robust phase boundaries in the MgSiO$_3$ phase diagram.

For stishovite, we found an accurate description for heat capacity and V–P–T data in the first sequence and by fitting its reference energy, we found a reasonable boundary between akimotoite and the two-phase field wadsleyite + stishovite, considering the small amount of points resulting from quench experiments. Two points belonging to the akimotoite field measured by Kanzaki (1987) at 1273 K are unavoidably inside our established ringwoodite + stishovite field. Representing these points better, invariably moves points belonging to field wadsleyite + stishovite measured by Sawamoto (1987) into the akimotoite field. The phase boundary between the phase fields akimotoite and wadsleyite + stishovite is almost horizontal due to anharmonicity of akimotoite. Negative anharmonicity increases heat capacity, and therefore entropy, relative to the quasi-harmonic approximation, its effect being larger at larger temperature and zero at zero temperature. That in turn results is a stronger decrease in the Gibbs energy of akimotoite relative to lower temperatures producing a flat behaviour of the phase boundary. The effect of anharmonicity on the 1 bar heat capacity of akimotoite in the temperature range of the measured data is, however, insignificant.

Because no heat capacity data are available for nonquenchable HPclinoenstatite, we used the descriptions of wadsleyite and stishovite to constrain the phase boundary

Table 3 Vibrational model parameters

	θ_1/K	$\Delta\theta/K$	γ_0	q_0	$a_0 \times 10^5 \, K^{-1}$	z_0	$n_{s.0}$
Fo	25.47 (37)	50.9405	1.114 (20)	1.53 (10)	−0.865 (460)	0.000	1.92 (13)
Fo(*)	25.47 (37)	50.9405	1.318 (20)	1.49 (10)	−0.865 (460)	0.000	1.92 (13)
			0.450 (20)	0.00	−0.865 (460)		
Wa	24.77 (67)	49.5416	1.260 (30)	1.00 (20)	−0.687 (290)	0.000	2.40 (13)
Ri	23.52 (67)	47.0372	1.250 (20)	1.00 (14)	0	0.000	2.19 (30)
Pc	17.05 (60)	34.0931	1.515 (30)	1.40 (14)	+0.911 (400)	7.30 (140)	2.07 (14)
St & St-I	24.86 (142)	49.7231	1.269 (70)	3.51 (40)	0	0.000	4.71 (100)
Si-II	24.84	49.6733	1.157 (70)	3.51 (40)	0	0	5.44 (100)
Pv	22.63 (179)	45.2499	1.403 (30)	0.19 (22)	−0.350 (300)	0.000	1.97 (30)
Pv(*)	22.64 (179)	45.2969	1.403 (30)	0.19 (22)	−0.350 (300)	0.000	1.97 (30)
Ppv	21.56 (200)	43.1232	1.535 (40)	1.36 (30)	0	0.000	2.20 (20)
Ppv(*)	21.35 (200)	42.7042	1.539 (40)	1.32 (30)	0	0.000	2.20 (20)
Aki	22.58 (267)	45.1531	1.290 (50)	0.42 (40)	−1.224 (300)	0.000	2.70 (50)
Mj	25.62 (300)	51.2332	1.430 (30)	0.000	0	0.000	0.61 (10)
			0.755				
Hcen	27.49 (18)	54.9718	1.157 (22)	0.57 (18)	−0.791 (300)	0.000	2.46 (7)
Lcen	27.67 (14)	55.0000	0.996 (50)	0.000	−1.223 (300)	0.000	1.69 (26)
Oen	28.81 (16)	57.6255	0.982 (30)	0.000	−1.059 (300)	0.000	1.69 (26)

Each polymorph is described with a 30-Einstein frequency model in which the Einstein temperatures at zero temperature and zero pressure are given by $\theta_k = \theta_1 + (k-1) \times \Delta\theta$, where k ranges from 1 to 30. For SiO$_2$-II, we used the same value for q as for stishovite. St-I denotes the CaCl$_2$ form of SiO$_2$ and is described with the same VDoS as stishovite. Dispersion in the Grüneisen parameters of forsterite, Fo(*), has been incorporated by two frequency ranges denoted by $k \in [1,17]$ and $k \in [18,30]$. For majorite, dispersion in Grüneisen parameters is incorporated in the two ranges $k \in [1,15]$ and $k \in [16,30]$

between this phase and wadsleyite + stishovite. This was achieved by fitting reference energy and anharmonicity parameter of HPclinoenstatite. The resulting description was used to constrain the phase boundaries between HPclinoenstatite and LPclinoenstatite and between LPclinoenstatite and orthoenstatite, which are not accurately determined experimentally, resulting in anharmonicity parameters of orthoenstatite and LPclinoenstatite.

Majorite was incorporated in the phase diagram by a small translational shift of the VDoS to within the uncertainty range of the DSC heat capacity measurements, and fitting its reference energy.

The phase boundary between perovskite and post-perovskite is uncertain, and it is discussed in "online resource, section Akimotoite, majorite and post-perovskite" and section "effect of pressure scales."

Uncertainties in model parameters given in Tables 2 and 3 are estimates. They are based on varying a single parameter outside the uncertainty range of the sum of squares due to experimental uncertainties in data sets we have found to be consistent with each other. These uncertainties are similar to reported experimental uncertainties. That also applies to shear modulus discussed in "online resource, section Shear modulus." Uncertainties in reference energy and anharmonicity parameters result from the second sequence, whereas those of other parameters are determined by the first sequence and insignificantly affected by the second sequence.

Effect of pressure scales

To bring coherence in the V–P–T measurements, we used a single pressure scale developed by Dorogokupets and Oganov (2007). The exception is MgO, for which our analysis is based on the primary pressure scale of Li et al. (2006), consistent with that developed by Kono et al. (2010). Our model for MgO is also consistent with ab initio predictions by Wu et al. (2008). It should be noted that the MgO description of Dorogokupets and Oganov (2007) does not represent the shock-wave data of Svendsen and Ahrens (1987) and those of Vassiliou and Ahrens (1981); their calculated Hugoniot is located between that calculated by the Debye model of Stixrude and Lithgow-Bertelloni (2011) and our own, plotted in "online resource Fig. 1." Therefore, for establishing pressures in V–P–T data which are based on a particular MgO scale, we could alternatively have proceeded by taking our own description for MgO in Tables 2 and 3. For pressures along the post-spinel and akimotoite–perovskite phase boundary, the pressure difference between our own MgO description and that of Dorogokupets and Oganov (2007) is insignificantly small, less than 0.2 GPa.

Table 4 Enthalpy differences in kJ/mol for reactions at 1 bar pressure in the system MgO–SiO$_2$

Nr	Transition	T/K	ΔH$^{this work}$	ΔH^{Debye,Fab}	ΔH^{exp}	References/combination
	Oxides → fo	298.15	−2174.894	−2028.903	−2173 ± 2	Robie and Hemingway (1995)
	Oxides → pc	298.15	−601.454	−560.968	−601.6 ± 0.3	Robie and Hemingway (1995)
	Oxides → oen	298.15	−1544.916	−1437.956	−1545.4 ± 1.5	Robie and Hemingway (1995)
1a	Fo → Wa	298	27.21 ± 1.0	25.45	27.2 ± 3.6	Akaogi et al. (2007)
b		975	27.13 ± 1.0	24.99	29.97 ± 2.84	Akaogi et al. (1989)
2a	Fo → Ri	298	37.75 ± 1.0	35.04	40.1 ± 3.1	Akaogi et al. (2007)
b		975	36.98 ± 1.0	33.04	39.05 ± 2.62	Akaogi et al. (1989)
3a	Wa → Ri	298	10.54 ± 0.54	9.59	12.9 ± 3.3	Akaogi et al. (2007)
b		975	9.84 ± 0.54	8.05	9.08 ± 2.12	Akaogi et al. (1989)
4a	Ri → Pc + Pv	298	86.30 ± 1.4	80.67	86.1 ± 3.6	Akaogi and Ito (1993a, b)
b		298			96.8 ± 5.8	Ito et al. (1990)
c		298			88.1 ± 4.7	[2a]+[5a]+[9a]
5a	Fo → Oen + Pc	298	28.52 ± 1.0	29.98	26.00 ± 2.52	Robie and Hemingway (1995)
b		970	28.62 ± 1.0	30.34	25.73 ± 1.19	Charlu et al. (1975)
6a	Oen → Mj	1000	35.41 ± 1.4	33.43	35.7 ± 3.0	Navrotsky (1995)
b		983	35.44 ± 1.4	33.24	30.80 ± 3.11	Yusa et al. (1993)
7	2Oen → Wa + St	986	69.18 ± 1.0	56.80	76.91 ± 7.69	Navrotsky et al. (1979)
8	2Oen → Ri + St	986	79.01 ± 1.0	64.83	81.80 ± 8.16	Navrotsky et al. (1979)
9a	Oen → Pv	298	95.52 ± 1.4	85.73	102.2 ± 2.5	Akaogi and Ito (1993a, b)
b		298		96.79$^{[Fab]}$	110.1 ± 4.1	Ito et al. (1990)
10a	Aki → Pv	298	48.47 ± 1.4	42.77	42.15 ± 2.05	Akaogi et al. (2002)
b		298		44.60$^{[Fab]}$	43.2 ± 5.0	Akaogi and Ito (1993a, b)
c		298			51.1 ± 6.6	Ito et al. (1990)
11a	Oen → Aki	298	47.06 ± 1.4	42.96	61.51 ± 1.99	Akaogi et al. (2002)
b		298		52.19$^{[Fab]}$	59.03 ± 4.26	Ashida et al. (1988)
12a	Mj → Aki	298	11.48 ± 1.4	9.54	26.3 ± 2.6	Akaogi et al. (2002)
b		983	12.04 ± 1.4	7.69	25.0 ± 5.3	Yusa et al. (1993)
c		298		18.90$^{[Fab]}$		
13a	Wa + St → 2Aki	986	25.76 ± 2.8	25.05	46.11 ± 7.94	[7]+[11a]
b		986		27.53$^{[Fab]}$	41.3 ± 10.9	[7]+[11b]
c		986			25.5 ± 10.9	[7]+[11c]
14a	Ri + St → 2Aki	986	15.94 ± 2.8	17.02	41.4 ± 8.4	[8]+[11a]
b		986		20.49$^{[Fab]}$	36.6 ± 11.3	[8]+[11b]
15a	Mj → Pv	298	59.95 ± 1.4	52.30	68.5 ± 3.2	Akaogi and Ito (1999)
b		298		63.50$^{[Fab]}$	66.5 ± 3.9	[6a]+[9a]

Label [Fab] denotes values resulting from the database of Fabrichnaya et al. (2004). Label 'exp' denotes values based on experimental work

Label 'Debye' in the enthalpy denotes the enthalpy difference calculated with the database of Stixrude and Lithgow-Bertelloni (2011)

Combination in the last column refers to combination of transitions in the first column

The difference between the two scales becomes significant above 40 GPa, affecting the analyses of perovskite and post-perovskite. Reanalysing the *V–P–T* data of Katsura et al. (2009a, b) for perovskite using our MgO description does not lead to significant differences in the model parameters as shown in Tables 2 and 3. However, for post-perovskite , our MgO description results in pressures about 6 GPa larger than reported by Guignot et al. (2007). Reanalyzing these

V–P–T data results in model parameters labelled as ppv(*) in Tables 2 and 3. That description produces values for ambient volume, bulk modulus and its pressure derivative of 24.71 cm^3/mol, 217 GPa and 4.35, respectively, consistent with predictions of Tsuchiya et al. (2005) using ab initio, 24.66 cm^3/mol, 216 GPa and 4.41, respectively. These values deviate from our description based on the pressure scale of Dorogokupets and Oganov (2007), 24.28 cm^3/mol,

Fig. 3 VDoS predicted by ab initio for wadsleyite and ringwoodite is described with 60 Einstein continua indicated by the *coloured rectangles*. The 60 Einstein monochromatic frequencies are placed in the middle of these continua. *Curves labelled* 'Debye' were calculated with the Debye model by Stixrude and Lithgow-Bertelloni (2011). Experimental data by Watanabe (1982) and Ashida et al. (1987) are below our calculated isochoric heat capacity for both polymorphs indicated by label C_v-60E. Labels C_p-60E and C_v-60E indicate isobaric and isochoric heat capacity calculated with a 60-Einstein frequency model
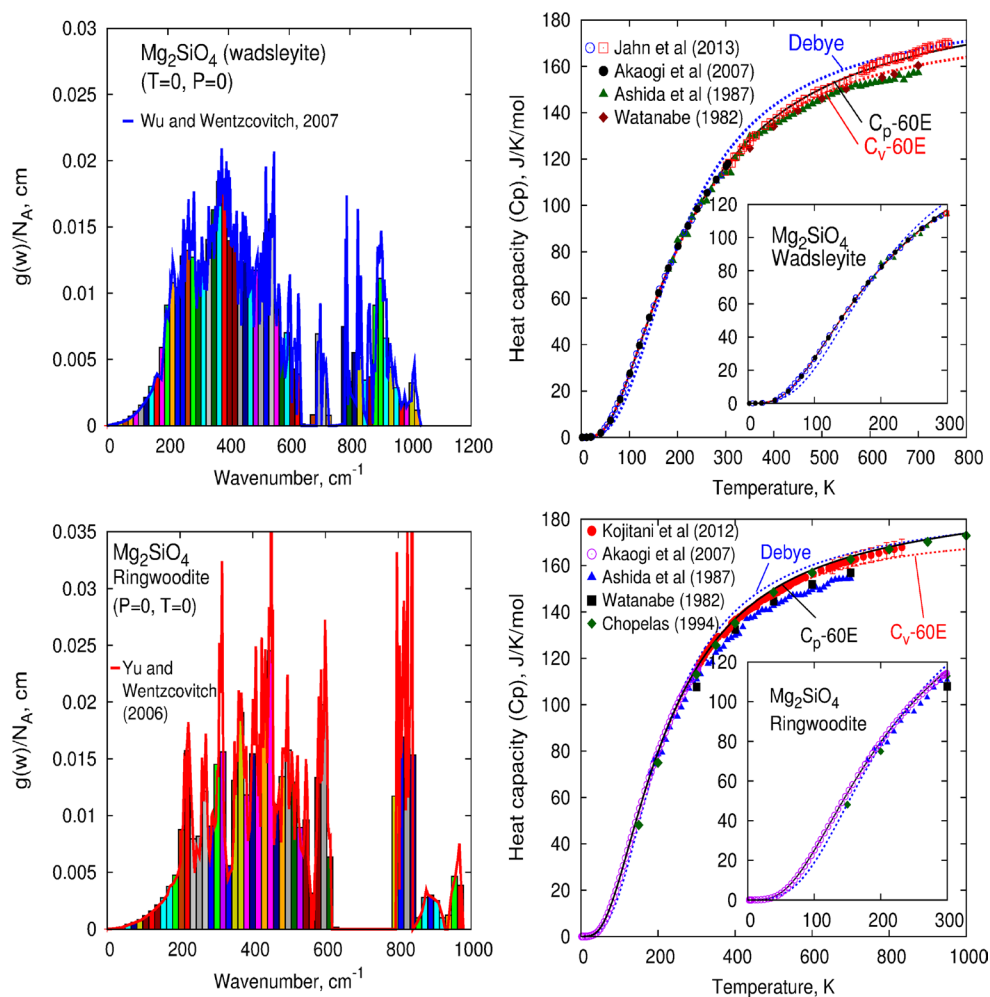
231 GPa and 4.25, respectively. The representation of isothermal bulk modulus predicted by Tsuchiya et al. (2005) in the temperature range between 0 and 4000 K and pressure range between 0 and 150 GPa improves by using our MgO description. The maximum deviation is 1 % and average deviation 0.3 %, smaller than our results based on the MgO scale of Dorogokupets and Oganov (2007), 7.5 and 3.2 %, respectively, see "online resource Table 2." The Clapeyron slope of the boundary between perovskite and post-perovskite resulting from this alternative description increases slightly to 10.1 ± 2.7 MPa/K. Because of the pressure scale-dependent description for post-perovskite, extrapolation to *P–T* conditions in the MgO + post-perovskite phase field, necessary for modelling heavy exoplanets, should be carried out cautiously.

Thermochemical data

Table 4 shows that heats of formation of forsterite, orthoenstatite and periclase resulting from our analysis represent

experimental values to within uncertainty. That also holds for enthalpy differences between phases in the system Mg$_2$SiO$_4$. For phases participating in the post-spinel transition, our analysis represents best the enthalpy difference determined by Akaogi and Ito (1993b). They measured the enthalpy difference between perovskite and orthoenstatite and followed the procedure of thermochemical cycles as indicated by transition (4c) of Table 4. Because they used older data in their calculations, we recalculated their enthalpy difference, 86.1 ± 3.6 kJ/mol, for the post-spinel phases with the more recent enthalpy data of Robie and Hemingway (1995) and Akaogi et al. (2007), resulting in a slightly larger but consistent value of 88.1 ± 4.7 kJ/mol.

Table 4 shows that enthalpy differences between orthoenstatite, wadsleyite, ringwoodite, majorite and stishovite, given by transitions (5) to (8) represent experimental data of difference sources to within experimental uncertainty. These data are therefore consistent with phase diagram data and thermophysical data. However, our calculated enthalpy differences related to orthoenstatite, akimotoite and perovskite in transitions (9), (10) and (11)

Fig. 4 *Solid curves* were calculated with a database in which the VDoS of each phase is represented with 60 Einstein frequencies. The *dashed curves* were calculated with a clone for which the VDoS of each endmember is represented by one single Einstein frequency. *Upper-left* Isotherms derived from a Debye model by Stixrude and Lithgow-Bertelloni (2011) are plotted as *grey curves*. Uncertainty in measurements is given by the symbol size. *Lower-left* The isotherm at 1073 K calculated with a Debye model by Stixrude and Lithgow-Bertelloni (2011) is plotted as the *grey curve*. When two adjacent symbols are plotted in the legend, the *left* one denotes the original pressure scale, the *right* one refers to the pressure scale of Dorogokupets and Oganov (2007). *Lower-right* we directed our optimization for SiO₂ (stishovite and I) by converting the pressures of the data of Andrault et al. (2003) to the platinum pressure scale of Dorogokupets and Oganov (2007) indicated by Pt-DO-07. Columbite, denoted as II, is stable above 85 GPa and volumes are plotted as the *dashed curve*
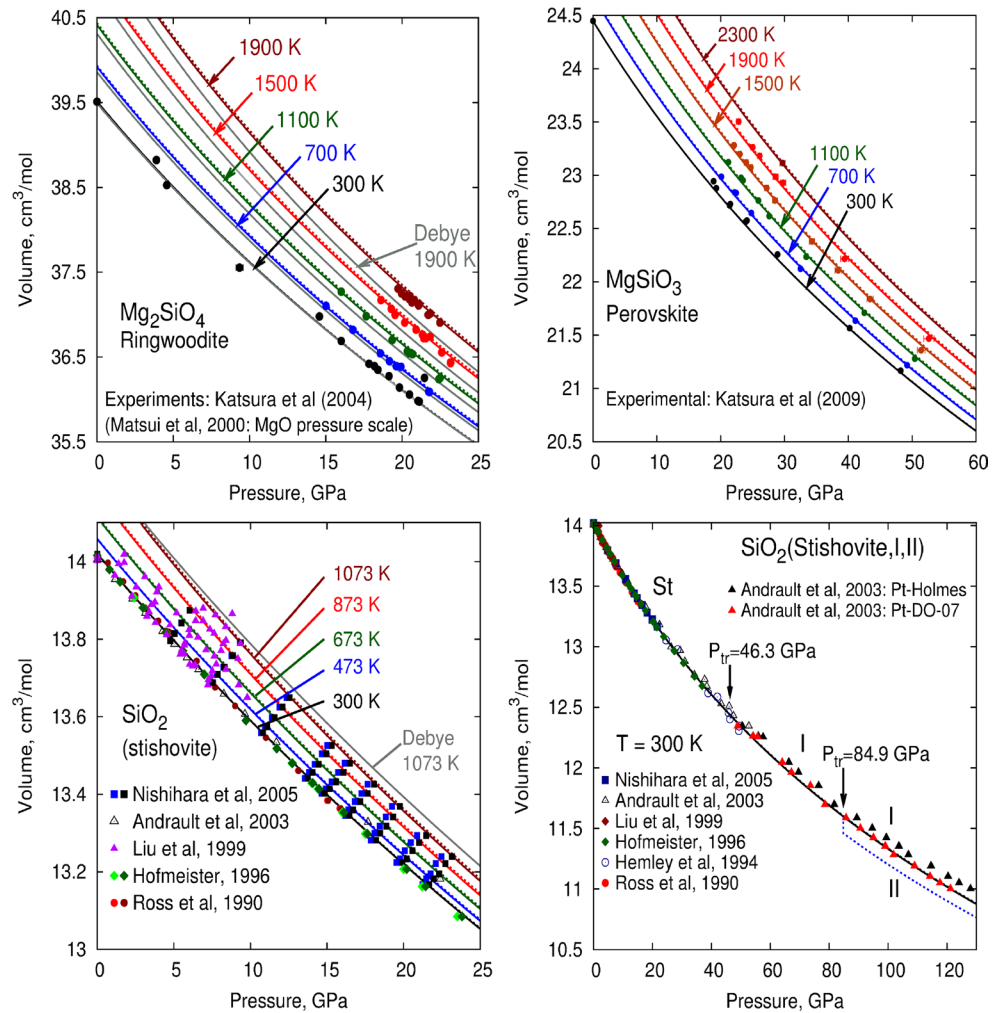
deviate significantly from experimentally established values. Experimental data for the enthalpy difference between perovskite and akimotoite are based on measurements of the enthalpy difference between perovskite and orthoenstatite, transition (9), and that between akimotoite and orthoenstatite, transition (11). For these two transitions, our calculated values are just as resulting from the databases of Stixrude and Lithgow-Bertelloni (2011) and Fabrichnaya et al. (2004) significantly smaller than the experimental values. Incorporating the experimental enthalpy differences in our database would require an enthalpy increase of perovskite by about 6 kJ/mol whereas that of akimotoite should increase with about 12 kJ/mol. However, incorporating these increments displaces our calculated akimotoite–perovskite phase boundary with about −3.4 GPa, resulting in a disappearance of the akimotoite phase field in the MgSiO₃ phase diagram, whereas the post-spinel phase boundary in the system Mg₂SiO₄ displaces by about 2.3 GPa to higher pressures. Alternatively, the Clapeyron slope of the akimotoite–perovskite phase boundary could be increased from −3.8 MPa/K to about −3.2 MPa/K, by increasing the entropy of akimotoite, either by shifting the frequencies in the VDoS or by changing the anharmonicity parameter. That increases the enthalpy difference between akimotoite and orthoenstatite from 47.07 kJ/mol to about 50 kJ/mol, but simultaneously the akimotoite field is replaced by the ringwoodite + stishovite field forming a triple point with perovskite at temperatures larger than 1400 K. That is in conflict with phase diagram points, reported by Kanzaki (1991) as akimotoite, plotted in Fig. 2 at 1273 K.

The deviations from the experimental values in transitions (9) and (11) also propagate in other transitions related to akimotoite and perovskite, such as in transitions (12) to (15), for which the three thermodynamic databases, including our own, recommend smaller values. The phase diagrams calculated from these databases apparently cannot be reconciled with the large experimental values for the enthalpy difference between orthoenstatite and akimotoite and between orthoenstatite and perovskite.

Changing the number of Einstein frequencies in a VDoS: database clones

In this section, we show a process to optimize the number of Einstein frequencies in a VDoS. In this process, we construct a new database from the original one in which all substances are described with the same but smaller number of Einstein frequencies. We call this new database a clone of the original one. We refer to this process as cloning a database because a large number of new databases can be formed with properties resembling that of the original one. Two requirements are necessary in this process.

The first requirement in this process is that all model parameters except frequencies, fractions in the VDoS and values for static volume remain unchanged. Therefore, the majority of model parameters remain unchanged. This requirement implies that we keep unchanged the value for the physical volume, V_0, at zero pressure and zero temperature. Because we change the VDoS, the value for thermal pressure at this condition will change, which must be counterbalanced by a change in the static pressure to match the external pressure. That is achieved by a change in the value for static volume, V_0^{st}, as can be deduced from Eq. (22) in our previous paper, Jacobs et al. (2013). In that equation, we replace the expression for the static pressure by Eq. (3) given in "Static lattice and vibrational properties" section of the present paper. Generally, only small changes of less than 0.1 % are required to counterbalance the change in thermal pressure in the procedure we describe below.

The second requirement is that we keep unchanged values for enthalpy and entropy resulting from the original database at a selected condition of pressure and temperature. By applying that constraint the entropy differences at the phase boundaries at that condition are exactly the same as resulting from the original database.

The first step in the procedure of making a clone of the original database starts by selecting the desired number of Einstein frequencies, N_E, for each substance. Next, we repeat the procedure of constructing the VDoS of each substance as described in Jacobs et al. (2013). For each substance, 60 Einstein frequencies with their corresponding values of the VDoS are available. Each VDoS in the original database is partitioned in N_E equidistant frequency ranges, for which the frequency interval is determined by the maximum frequency.

In the second step, a condition of pressure and temperature is selected for which the value of entropy of each substance is the same as resulting from the original database. We call that condition a target condition. To keep Clapeyron slopes of phase boundaries depicted in Figs. 1 and 2 at about the same values, one could use for instance the triple point between orthoenstatite, LPclinoenstatite and HPclinoenstatite to make sure that the small entropy and volume

differences between these phases are retained. To keep the entropy of a specific substance at the same value as resulting from the original database at the target condition, all Einstein frequencies of that substance are multiplied with a common factor, resulting in an expansion or contraction of the VDoS. Values for this common factor are typically about 1±0.002 for the 30-Einstein clone we used in Table 3 and are obtained by an optimization process. Generally, values larger than one result in smaller entropy at the target condition and vice versa.

In the last step, we change the value for the reference energy of each substance, U^{ref}, in Eq. (1) such that the enthalpy at the target condition is identical with that resulting from the original database. That ensures that the Gibbs energy at the target condition remains unchanged.

It is evident that employing a smaller number of Einstein frequencies results in a loss of details in the VDoS. Therefore, representing thermodynamic data will be less accurate. The most extreme case is representing the VDoS by only one Einstein frequency and the examples in "online resource Fig. 2" show that the resulting heat capacity mismatches the experimental data. However, the single Einstein model is instructive to show that although calculated heat capacities mismatch experimental data, other thermodynamic properties can be represented quite accurately. We shall demonstrate this with the help of Table 5 for ringwoodite. Table 5 shows that changing the original description of ringwoodite to a single Einstein model results in a change in the vibrational contribution to pressure, P^{vib}, of about 0.2 GPa, which is counterbalanced at zero total pressure by the same amount in static pressure, −0.2 GPa. That is achieved by a small change in static volume of about 0.1 %, as shown in the header of Table 5. The reason that we keep V_0 unchanged is that thermal expansivity is small at low temperature, resulting in about the same volumes as in the original description for ringwoodite at low temperatures. Therefore, the volume difference relative to the original description at 300 K is small, about only 0.004 % as indicated in Table 5. At high temperature, e.g. 2000 K, when vibrational modes become saturated, isochoric heat capacity approaches the $3nR$ Dulong–Petit limit and vibrational contribution to energy, U^{vib}, approaches the value $3nRT$. Therefore, these properties are much less sensitive to the VDoS than at low temperature. Because the vibrational contribution to pressure is related to U^{vib}, as $P^{vib} = \gamma U^{vib}/V$, also that property becomes less sensitive to the VDoS at high temperature. For that reason, the difference in P^{vib} at high temperature, between the two Einstein models is much smaller than at 300 K. Table 5 shows that this is only 0.3 % at 2000 K. The maximum volume difference at any temperature between the two Einstein models is of the same magnitude as the difference between the static volumes. That is illustrated as follows. At extremely high temperature, P^{vib}

Table 5 Thermodynamic properties for ringwoodite calculated with a 60-Einstein model and with a 1-Einstein model at zero pressure

T/K	N_E	P^{vib}	V	K^{st}	K^{vib}	K	α	C_V	C_P	S
0	60	1.911	39.404	183.67	2.39	186.06	0	0	0	0
	1	1.720	39.404	184.48	2.15	186.63	0	0	0	0
	Dev %	−9.99	0	0.44	−10	0.31	0	0	0	0
300	60	2.410	39.512	181.55	1.63	183.18	1.99	114.93	115.79	83.82
	1	2.213	39.510	182.38	1.28	183.66	2.14	123.90	124.90	76.13
	Dev %	−8.158	−0.004	0.46	−21.5	0.27	7.54	7.80	7.87	−9.17
2000	60	11.237	41.730	142.76	−1.39	141.37	3.90	172.85	190.74	391.75
	1	11.202	41.763	142.92	−1.51	141.41	3.91	173.40	191.43	392.47
	Dev %	−0.308	0.080	0.11	8.63	0.03	0.30	0.32	0.39	0.18

For the 1-Einstein model we used (1173 K, 1 bar) as target condition. The static volume resulting from the 60-Einstein model is 39.005 cm^3/mol and that of the 1-Einstein model is 39.045 cm^3/mol. Units are: volume, cm^3/mol, vibrational pressure, static and vibrational bulk modulus, GPa, thermal expansivity, 10^{-5} K^{-1}, isochoric and isobaric heat capacity, and entropy, JK^{-1} mol^{-1}. Deviations are given in per cent

is independent of the VDoS and therefore, the volume compression in the expression for the static pressure calculated from the original description must be equal for both Einstein models. Denoting the volume and static volume of the original description by V_m and $V^{st}_{0,m}$, that of the 1-Einstein description by V_c and $V^{st}_{0,c}$ and the static volume difference between the two Einstein models by Δ, we have:

$$\frac{V_m}{V^{st}_{0,m}} = \frac{V_c}{V^{st}_{0,c}} = \frac{V_c}{V^{st}_{0,m} + \Delta} \text{ or } V_c = V_m + \frac{V_m}{V^{st}_{0,m}}\Delta \qquad (22)$$

Generally, the ratio of volume and static volume is small, typically 1.07 at 2000 K and 1.12 at 3000 K, and Eq. (22) shows that at high temperature the volume difference calculated from the two models is of the same magnitude as the static volume difference. When the number of Einstein frequencies increases, the difference between the static lattice volume of the original description and that of the clone, rapidly decreases in absolute value. For a 2-Einstein model, this difference is 0.05 %; for a 4-Einstein model, it is 0.03 %.

The single Einstein model contains an interesting feature, which was a point of discussion at the time Einstein launched his model, namely that predicted isochoric heat capacity is invariantly too small relative to experimental data at very low temperature. We shall use this feature to demonstrate that volume differences between phases participating in equilibria calculated by the clone do not change significantly from that of the original database. That appears to be the case for all substances in our database, as illustrated for some of them in "online resource Fig. 2." Because of that feature, also predicted vibrational energy is too small relative to the original description. That in turn leads to smaller vibrational pressure, $P^{vib} \approx \gamma_0 U^{vib}/V_0$, relative to the original description. Because the vibrational pressure is positive, as indicated in Table 5, the static pressure must be negative to match the external pressure.

The 1-Einstein model therefore predicts static pressures which are less negative relative to the original description. Because the value of the physical volume V_0 remains unchanged and the static pressure versus volume curve of the 1-Einstein description is displaced upward in pressure, the static volume must be larger than that of the original description. That feature is quite important, because it holds for all substances in the small database we present here. Using Eq. (22), the volume of a substance at high temperature calculated with a 1-Einstein model is also larger than that of the original description. Additionally, we found that the volume change at high temperature appears to be of the same order of magnitude for all substances. For phase boundaries located at high pressures, this characteristic is important because it indicates that volume differences between different substances calculated with a 1-Einstein model will not be very different relative to those calculated by the original description. The reason that this holds true is that bulk modulus is relatively insensitive in the cloning process. Table 5 shows that at low temperature, the effect of the VDoS is largest for the vibrational contribution to bulk modulus, K^{vib}. However, this contribution is quite small compared to the static bulk modulus, K^{st}. The last property is affected by only about 0.4 %, and as a result the total bulk modulus changes only by 0.3 %. The vibrational contribution to bulk modulus can be written in terms of C_v and U^{vib}. At high temperature, where the effect of the VDoS becomes smaller, the difference in K^{vib} between the two Einstein models will become smaller as temperature increases. At high temperature, the compression term in the static bulk modulus converges to the same value, resulting in about the same total bulk modulus for the two models. Also thermal expansivity difference between the two models becomes smaller at high temperature because this property can be written as $\alpha = \gamma C_v/(KV)$. Because at high temperature, the difference in isochoric heat capacity,

Table 6 Ambient entropy values, in JK^{-1}mol^{-1}, calculated with different database clones

	$S_{298.15}^{60}$	$S_{298.15}^{30}$	$S_{298.15}^{10}$	$S_{298.15}^{5}$	$S_{298.15}^{[F]}$	$S_{298.15}^{exp}$	References
Fo	93.99	94.01	94.20	95.37	95.60	94.0 ± 0.1	Dachs et al. (2007)
Wa	86.72	86.72	86.78	87.49	95.00	86.4 ± 0.4	Akaogi et al. (2007)
Ri	83.11	83.06	83.20	83.83	90.60	82.7 ± 0.5	Akaogi et al. (2008)
Pc	26.90	26.90	26.92	27.05	26.94	26.924 ± 0.08	Chase et al. (1985)
St	24.75	24.77	24.76	24.92	24.64	24 ± 0.03	Akaogi et al. (2011)
						24.94 ± 0.10	Yong et al. (2012)
SiO$_2$-II	22.89	22.90	22.95	23.22	–	–	–
Pv	57.90	57.92	57.97	57.90	63.60	57.9 ± 0.3	Akaogi et al. (2008)
PPv	55.58	55.60	55.72	55.79	–	–	–
Aki	53.41	53.44	53.62	54.11	58.30	53.7 ± 0.4	Akaogi et al. (2008)
Mj	66.12	66.08	66.13	67.10	60.30	–	–
HCen	63.70	63.73	63.80	64.92	65.30	–	–
LCen	65.62	65.64	65.77	66.78	–	65.63 ± 0.023	Drebushchak et al. (2008)
Oen	66.49	66.52	66.53	67.61	66.27	66.27 ± 0.10	Krupka et al. (1985)

The number of frequencies in the VDoS are indicated as superscripts in the entropy. Label 'exp' denotes the experimental value including its uncertainty. Label [F] denotes entropies are taken from Fabrichnaya et al. (2004)

volume, bulk modulus and thermal expansivity between the two models become smaller also the difference in isobaric heat capacity becomes smaller. In Table 5, we used as target condition 1173 K and 1 bar to construct the 1-Einstein model. Selecting a high temperature is advantageous because in this case the entropy at 1173 K for ringwoodite is the same as for the original description, even when heat capacity below this temperature is significantly different. The calculation of entropy at temperatures above 1173 K is considered as the integral over the C_P/T function, which is split into two temperature ranges. In the first range between 0 and 1173 K, the result of that integration is the same as that for the original description and in the second range, the integration takes place over C_P/T where C_P is not significantly different from the original description. For that reason, the entropy difference between the two Einstein models becomes smaller at high temperature as indicated in Table 5. Because this characteristic does not change at large pressure, volume difference and entropy difference in Clapeyron slopes calculated with a 1-Einstein database will not be very different from those calculated from the original database.

We cloned the original database to one in which all substances are described with a 1-Einstein model and compared results obtained with the two databases. Because entropy differences between orthoenstatite, LPclinoenstatite and HPclinoenstatite are very small, we have set as target condition (1173 K, 7.9 GPa) to match the triple point between these phases as calculated from the original database. That has no effect on values in Tables 5 and 6. Figures 1 and 2 show that the difference between phase boundaries obtained with the two databases is remarkably small, typically less than about 0.2 GPa. That even holds for phase boundaries at temperatures far below 1173 K, as indicated by Fig. 2 and at extreme pressures above 100 GPa for the phase boundary between perovskite and post-perovskite. Figures 4 and 5 show for ringwoodite, perovskite, stishovite and post-perovskite that volumes in wide ranges of pressure and temperature calculated with the two databases are insignificantly different relative to experimental uncertainties. That also applies to bulk modulus and shear modulus as demonstrated in Fig. 5 for orthoenstatite. Figure 5 shows for HPclinoenstatite that accurate shear velocity measurements of Kung et al. (2005) are less well represented by a 1-Einstein model, especially at low temperature. As demonstrated in Fig. 6, five or more Einstein frequencies are necessary to represent these data with an average deviation of 0.1 %.

Special care must be taken when dispersion in Grüneisen parameters is needed in the description, such as for majorite. Because the 1-Einstein model, just as the Debye model contains only one Grüneisen parameter, it is unable to incorporate this feature. In our cloning process, we have averaged the Grüneisen parameters of the original description of majorite, resulting in a value of 1.1, which appears to be too small for representing thermal expansivity and phase boundaries in which majorite is involved. Therefore, we fine-tuned the Grüneisen parameter to a value of 1.16 and additionally the reference energy. Figures 2 and 5 show that phase diagram and thermal expansivity are almost indistinguishable from that resulting from the original description. Because we modelled dispersion in Grüneisen parameters in only two frequency ranges, Einstein models for majorite in which $N_E > 1$ do not require a

Fig. 5 *Solid curves* were calculated with the database in which the VDoS of each phase is represented with 60 Einstein frequencies. The *dashed curves* were calculated with a clone for which the VDoS of each phase is represented by one Einstein frequency. *Lower-right* a single Einstein frequency is insufficient to describe the shear sound velocity data to within experimental uncertainty; at least five Einstein frequencies are required to represent these data to within 0.1 % uncertainty, see Fig. 6
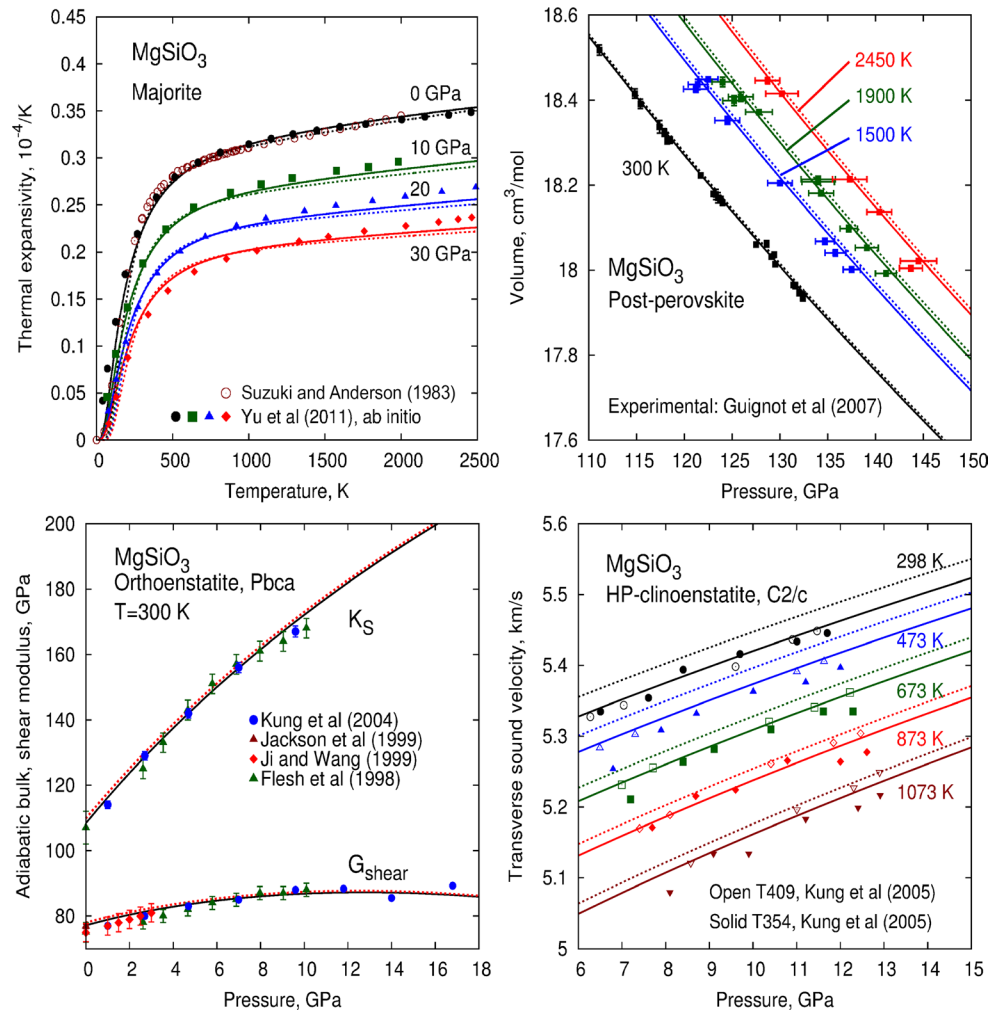

fine-tuning in the model parameters. However, we anticipate that for substances requiring dispersion in Grüneisen parameters in more than two frequency ranges more complicated adjustments are necessary.

The conclusion of our comparison of the two models is that a 1-Einstein model cloned from the original database represents well experimental data of all substances except heat capacity and entropy at low temperatures and shear sound velocity for HPclinoenstatite. Generally, such a 1-Einstein model even represents better *V–P–T* data than a Debye model such as demonstrated for ringwoodite and stishovite in Fig. 4.

We now turn to the question how many Einstein frequencies are necessary to represent experimental data including heat capacity. The answer to that question depends on the application. For low-temperature applications larger numbers are required than for high-temperature applications. In most thermodynamic databases, nowadays applied in materials science, heat capacity is described accurately only for temperatures above room temperature. To have an indication of how many Einstein frequencies are necessary in such

a case, we used the same target condition (1173 K, 7.9 GPa) as before and compared the values of ambient entropy for all substances calculated with the original database and the clone. Figure 6 shows, for some examples, that the required number of Einstein frequencies is much smaller than 60 to represent experimental entropy values to within their uncertainties. This number depends strongly on the experimental technique that has been applied to establish the entropy. For LPclinoenstatite, the entropy has been determined with adiabatic calorimetry, which is generally more accurate than the PPMS technique used for wadsleyite and perovskite, and therefore requires a larger number of Einstein frequencies, 20 in this case. For forsterite, a minimum of 14 Einstein frequencies are required in its VDoS. Table 6 shows that for most substances about 10 Einstein frequencies are required to represent room-temperature entropy data. That appears to be sufficient to represent all thermodynamic and shear modulus data above room temperature to within their experimental uncertainties. At temperatures below 300 K, the representation of heat capacity data remains remarkably good for all substances. For instance at 100 K,
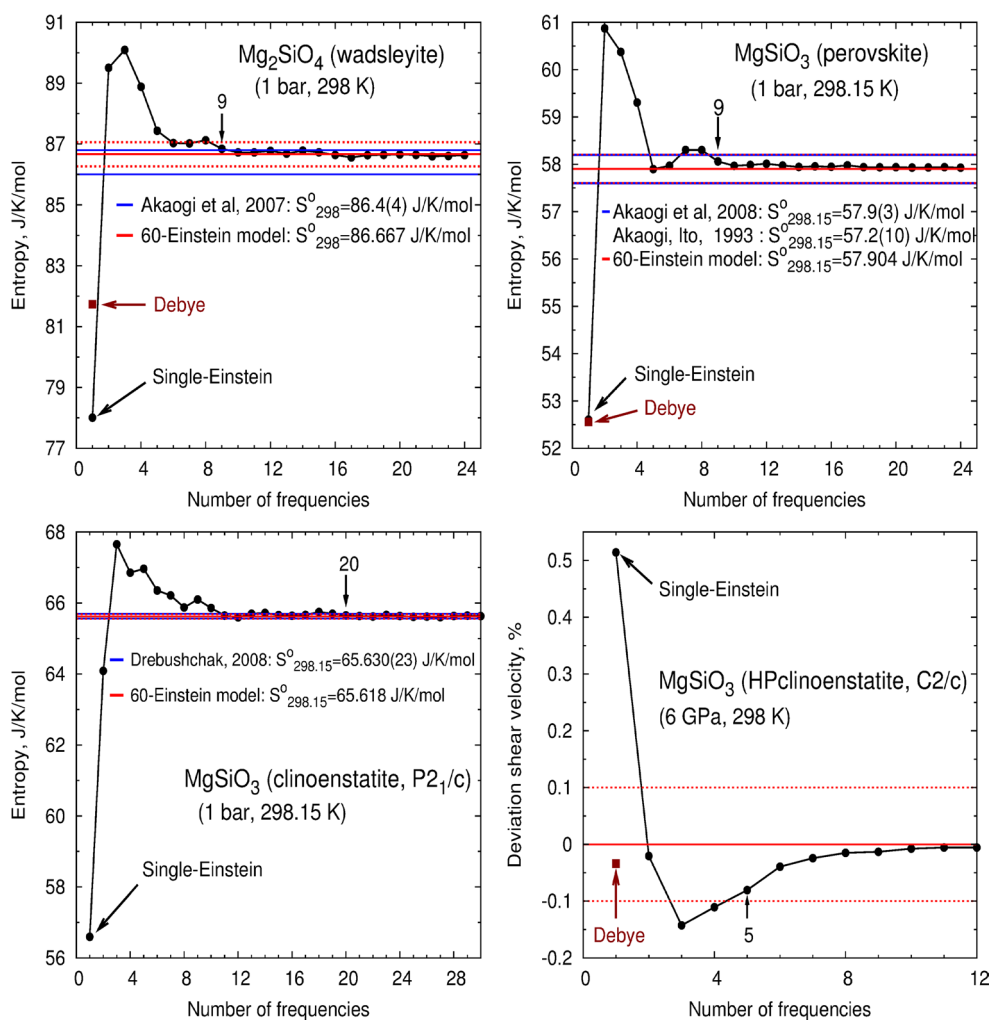
Fig. 6 *Upper-left* and *upper-right* clones with nine Einstein frequencies or more produce values for ambient entropy of wadsleyite and perovskite insignificantly different from the original database. *Lower-left* because the uncertainty of 0.035 % in the ambient entropy of low-pressure clinoenstatite is much smaller than for wadsleyite, 0.46 %, 20 Einstein frequencies are needed. *Lower-right* at least five Einstein frequencies are required to describe shear sound velocity with aver- age deviation of 0.1 % compared to that of the original database (see *lower-right* frame of Fig. 5). The experimental value including its uncertainty in all plots is indicated by the *solid blue curves* whereas the value calculated with a 60-Einstein model including the same uncertainty is given by the *solid* and *dashed red curves*. The label Debye gives entropy and sound velocity values calculated with the database of Stixrude and Lithgow-Bertelloni (2011)

entropies generally deviate less than 3 % for a 10-Einstein clone and less than 0.5 % for a 30-Einstein clone. Table 6 shows that our method results in more accurate entropy values for most substances relative to those resulting from the database of Fabrichnaya et al. (2004). This is mainly due to our method's ability to discriminate between different heat capacity data sets as discussed in "online resource, section Heat capacities." The exception is orthoenstatite, for which the VDoS of Choudhury and Chaplot (2000) results in a small overestimation of heat capacity at temperatures below 100 K, which cannot be compensated by a simple shift in the frequencies of the VDoS. Obtaining a near perfect description of the heat capacity requires changing fractions of the VDoS, keeping all other model parameters unchanged. In that case, resulting phase equilibria between LPclinoenstatite, HPclinoenstatite and orthoenstatite are insignificantly different from our previous calculations, indicating that our calculated entropy for orthoenstatite, using the VDoS of Choudhury and Chaplot (2000), is reasonable for temperatures above 800 K.

Conclusions

We showed that incorporating a VDoS predicted by ab initio into our method is a successful way to develop an accurate database for calculating thermodynamic properties and the shear modulus of substances in large ranges of

pressures and temperatures. Moreover, we showed that our method can be used to discriminate heat capacities, which is useful for making decisions which data set should be used in a thermodynamic analysis. Because of this characteristic, our method offers an extra tool to constrain location and Clapeyron slope of phase boundaries relative to a Debye method or methods that depend on parameterizations of the Gibbs energy. Additionally, this characteristic results in more accurate room-temperature entropies for most substances relative to these methods. The exception is orthoenstatite for which the VDoS of Choudhury and Chaplot (2000) results in an overestimation of heat capacity between 0 and 100 K and therefore an overestimation of entropy at ambient conditions. However, fine-tuning heat capacity by changing the VDoS does not have a significant effect on phase equilibria between orthoenstatite, HPclinoenstatite and LPclinoenstatite. We recommend re-establishing a VDoS for orthoenstatite.

Data for heat of formation and enthalpy difference for most transitions are represented to within experimental uncertainty. The exceptions are those between orthoenstatite and akimotoite and between orthoenstatite and perovskite at room temperature and 1 bar pressure, which cannot be reconciled with the phase diagrams for Mg_2SiO_4 and $MgSiO_3$.

To avoid inconsistencies and to enhance transparency in our analysis of V–P–T data, we used one pressure scale for all substances, that of Dorogokupets and Oganov (2007). By using this scale, we showed for the stishovite and the $CaCl_2$ form of SiO_2 that the second-order transition between them has a much smaller effect on volume than derived by Andrault et al. (2003). An additional feature of using a single pressure scale is that performing future improvements of our database is much simpler when pressure scales become more accurate.

For MgO, we arrived at the same conclusion as Wu et al. (2008) by ab initio that shock-wave data of Svendsen and Ahrens (Svendsen and Ahrens 1987) are represented well when the room-temperature isotherm is based on the primary pressure scale of Li et al. (2006). Because the MgO description of Dorogokupets and Oganov (2007) represents these shock-wave data less well, our model can be used as an alternative pressure scale, but it results in pressures about 6 GPa larger at pressures between 100–140 GPa. In that case for post-perovskite, better consistency is achieved between the experimental V–P–T data of Guignot et al. (2007) and bulk modulus in P–T space predicted by Tsuchiya et al. (2005) using ab initio.

Our small database can be cloned to databases in which the VDoS of substances are described with arbitrary smaller number of Einstein frequencies, using an automated process. This is useful in cases when a simpler thermodynamic description is desired that enhances computational efficiency or to make comparisons with methods employing a simplified VDoS. We showed that the VDoS has a large effect on heat capacity and entropy, but that its effect on volume properties is small. The process of cloning a database is more efficient than performing new thermodynamic analyses with smaller number of Einstein frequencies. We showed that a database clone in which the VDoS of each substance is described with a single Einstein frequency achieves remarkable precise phase diagrams for which phase boundaries deviate less than 0.2 GPa relative to those calculated with the original database. Such database also achieves remarkable precision for volume, bulk modulus, thermal expansivity and shear modulus relative to experimental uncertainties in wide ranges of pressure and temperatures. However, heat capacity and therefore entropy and enthalpy are not represented well, and in the case of HPclinoenstatite transverse sound velocity in P–T space is not represented well. Additionally, substances requiring dispersion in Grüneisen parameters in their description, such as forsterite and majorite, should be treated with care when a small number of Einstein frequencies are employed. In such cases, modifications of model parameters are required to achieve a desired accuracy for phase diagrams and thermodynamic properties. We found that for most substances in the system MgO–SiO_2, a minimum of 10 Einstein frequencies is necessary to represent heat capacity sufficiently accurate. However, larger numbers are required in cases when accurate calorimetric data are available such as for LPclinoenstatite and forsterite.

Calculations in this work were performed with program XiPT written in Pascal, Jacobs and Oonk (2012). To make our multi-Einstein method more transparent and to enhance incorporating it in other software, we made available software codes written in Fortran and FreePascal. This software enables calculating thermodynamic properties of substances in P–T space, using input data files for the substances treated in the present work. The software and input data files can be downloaded from website http://www.geo.uu.nl/~jacobs/Downloads.

References

Akaogi M, Ito E (1993a) Heat capacity of $MgSiO_3$ perovskite. Geophys Res Lett 20:105–108

Akaogi M, Ito E (1993b) Refinement of enthalpy measurement of $MgSiO_3$ perovskite and negative pressure. temperature slopes for perovskite-forming reactions. Geophys Res Lett 20:1839–1842

Akaogi M, Ito E (1999) Calorimetric study on majorite-perovskite transition in the system $Mg_4Si_4O_{12}$–$Mg_3Al_2Si_3O_{12}$: transition boundaries with positive pressure-temperature slopes. Phys Earth Plan Int 114:129–140

Akaogi M, Ito E, Navrotsky A (1989) Olivine-modified spinel-spinel transitions in the system Mg_2SiO_4–Fe_2SiO_4: calorimetric measurements, thermochemical calculation, and geophysical application. J Geophys Res 94:15671–15685

Akaogi M, Tanaka A, Ito E (2002) Garnet-ilmenite-perovskite transitions in the system $Mg_4Si_4O_{12}$–$Mg_3Al_2Si_3O_{12}$ at high pressures and high temperatures: phase equilibria, calorimetry and implications for mantle structure. Phas Earth Plan Int 132:303–324

Akaogi M, Takayama H, Kojitani H, Kawaji H, Atake T (2007) Low-temperature heat capacities, entropies, and enthalpies of Mg2SiO4 polymorphs, and α-β-γ and post-spinel phase relations at high pressure. Phys Chem Minerals 34:169–183

Akaogi M, Kojitani H, Morita T, Kawaji H, Atake T (2008) Low-temperature heat capacities, entropies and high-pressure phase relations of $MgSiO_3$ ilmenite and perovskite. Phys Chem Minerals 35:287–297

Akaogi M, Oohata M, Kojitani H, Kawaji H (2011) Thermodynamic properties of stishovite by low-temperature heat capacity measurements and the coesite-stishovite transition boundary. Am Mineral 96:1325–1330

Anderson OL (1998) Equation of state of solids for geophysics and ceramics. Oxford monographs on geology and geophysics. Oxford University Press, New York, p 163

Andrault D, Angel RJ, Modenfelder L, Bihan T (2003) Equation of state of stishovite to lower mantle pressures. Am Mineral 88:301–307

Angel RJ, Hugh-Jones DA (1994) Equations of state and thermodynamic properties of enstatite pyroxenes. J Geophys Res 99:19777–19783

Ashida T, Kume S, Ito E (1987) Thermodynamic aspects of phase boundary among α-, β-, and γ-Mg2SiO4. In: Manghnani MH, Syono Y (eds) High-pressure research in mineral physics. Terra Scientific Publishin Company (TERRAPUB), Tokyo/American Geophysical Union, Washington, D.C, pp 269–274

Ashida T, Kume S, Ito E, Navrotsky A (1988) $MgSiO_3$ ilmenite: heat capacity, thermal expansivity and enthalpy of transformation. Phys Chem Minerals 16:239–245

Boehler R, Chopelas A (1991) A new approach to laser heating in high pressure mineral physics. Geophys Res Lett 18:1147–1150

Carpenter MA (1992) Thermodynamics of phase transitions in minerals: a macroscopic approach. In: The stability of minerals, Price GD, Ross NL (eds) Chapman & Hall, London, ISBN 0412441500

Charlu TV, Newton RC, Kleppa OJ (1975) Enthalpies of formation at 970 K of compounds in the system MgO–Al_2O_3–SiO_2 from high temperature solution calorimetry. Geochim Cosmochim Acta 39:1487–1497

Chase Jr MW, Davies CA, Downey Jr JR, Frurip DJ, McDonald RA, Syverud AN (1985) JANAF thermochemical tables. J Phys Chem Ref Data Suppl 1(14):1469

Chopelas A, Boehler R, Ko T (1994) Thermodynamics and behavior of & γ-Mg2SiO4 at high pressure: implications for Mg_2SiO_4 phase equilibrium. Phys Chem Minerals 21:351–359

Choudhury N, Chaplot SL (2000) Free energy and relative stability of the enstatite $Mg_2Si_2O_6$ polymorphs. Solid State Comm 114:127–231

Chudinovskikh L, Boehler R (2004) $MgSiO_3$ phase boundaries measured in the laser-heated diamond anvil cell. Earth Planet Sci Lett 219:285–296

Dachs E, Geiger CA, Seckendorff von V, Grodzicki M (2007) A low-temperature calorimetric study of synthetic (forsterite +

fayalite) $\{Mg_2SiO_4 + Fe_2SiO_4\}$ solid solutions: An analysis of vibrational, magnetic, and electronic contributions to the molar heat capacity and entropy of mixing. J Chem Thermodyn 39:906–933

Dorogokupets PI, Oganov AR (2007) Ruby, metals, and MgO as alternative pressure scales: a semiempirical description of shock wave, ultrasonic, x-ray, and thermochemical data at high temperatures and pressures. Phys Rev B 75(024115):1–6

Drebushchak VA, Kovalevskaya YA, Paukov IE, Surkov NV (2008) Low-temperature heat capacity of monoclinic enstatite. J Thermal Analysis and Calorimetry 94:493–497

Fabrichnaya O, Saxena SK, Richet P, Westrum EF Jr (2004) Thermodynamic data, models, and phase diagrams in multicomponent oxide systems. Springer-Verlag, New York

Fei Y, Bertka CM (1999) Phase transformations in the Earth's mantle and mantle mineralogy. In: Fei Y, Bertka CM, Myssen BO (eds) Mantle petrology: field observations and high pressure experimentation, vol 6. The Geological Society, Washington, DC, pp 189–207

Fei Y, Orman J, Li J, van Westrenen W, Sanloup C, Minarik W, Hirose K, Komabayashi T, Walter M (2004) Experimentally determined postspinel transformation boundary in Mg_2SiO_4 using MgO as an internal pressure standard and its geophysical implications. J Geophys Res B 109:B02305

Flesh LM, Li B, Liebermann RC (1998) Sound velocities of polycrystalline $MgSiO_3$-orthopyroxene to 10 GPa at room temperature. Am Miner 83:444–450

Gasparik T (2003) Phase diagrams for geoscientists. Springer-Verlag, Berlin Heidelberg New York

Ghiorso MS (2004) An equation of state for silicate melts. I. Formulation of a general model. Am J Sci 304:637–678

Gillet P, Richet P, Guyot F, Fiquet G (1991) High-temperature thermodynamic properties of forsterite. J Geophys Res B 96:11805–11816

GilletP Daniel I, Guyot F, Matas J, Chervin J-C (2000) A thermodynamic model for $MgSiO_3$-perovskite derived from pressure, temperature and volume dependence of Raman mode frequencies. Phys Earth Planet Int 117:361–384

Guignot N, Andrault D, Morard G, Bolfan-Casanova N, Mezouar M (2007) Thermoelastic properties of post-perovskite phase $MgSiO_3$ determined experimentally at core-mantle boundary P–T conditions. Earth Plan Sci Lett 256:162–168

Hemley RJ, Prewitt CT, Kingma KJ (1994) In Silica: physical behavior, geochemistry and materials applications. Heaney PJ, Prewitt CT, Gibbs GV (eds) Mineralogical Society of America, Washington, DC, pp 41–81

Hemley RJ, Shu J, Carpenter MA, Hu J, Mao HK, Kingma KJ (2000) Strain/order coupling in the ferroelastic transition in dense SiO_2. Solid State Comm 114:527–532

Hirose K, Komabayashi T, Murakami M, Funakoshi K-I (2001) In situ measurement of the majorite-akimotoite-perovskite phase transition boundaries in $MgSiO_3$. Geophys Res Lett 22:4351–4354

Hofmeister AM (1996) Thermodynamic properties of stishovite at mantle conditions determined from pressure variations of vibrational modes. In: Dyar MD, McCammon C, Schaefer MW (eds) Mineral spectroscopy: a tribute to Roger G Burns. The Geochemical Society, Special Publication No 5, 1996

Holland TJB, Powel R (1998) An internally consistent thermodynamic data set for phases of petrological interest. J Metamorphic Geol 16:309–343

Inoue T, Irifune T, Higo Y, Sanchira T, Sueda Y, Yamada A, Shinmei T, Yamazaki D, Ando J, Funakoshi K, Utsumi W (2006) The phase boundary between wadsleyite and ringwoodite in Mg_2SiO_4 determined by in situ X-ray diffraction. Phys Chem Minerals 33:106–114

Ito E, Navrotsky A (1985) MgSiO3 ilmenite: calorimetric, phase equilibria, and decomposition at atmospheric pressure. Am Mineral 70:1020–1026

Ito E, Takahashi E (1989) Postspinel transformation in the system Mg2SiO4–Fe2SiO4 and some geophysical implications. J Geophys Res B 94:10637–10646

Ito E, Akaogi M, Topor L, Navrotsky A (1990) Negative pressure–temperature slopes for reactions forming MgSiO3 perovskite from calorimetry. Science 249:1275–1278

Jackson JM, Sinogeikin SV, Bass JD (1999) Elasticity of MgSiO3 orthoenstatite. Am Miner 84:677–680

Jacobs MHG, de Jong BHWS (2007) Placing constraints on phase equilibria and thermo-physical properties in the system MgO–SiO2 by a thermodynamically consistent vibrational method. Geochim Cosmochim Acta 71:3630–3655

Jacobs MHG, Oonk HAJ (2012) Equilibrium between phases of matter. Supplemental text for material science and high-pressure geophysics, Springer

Jacobs MHG, Schmid-Fetzer R, van den Berg AP (2013) An alternative use of Kieffer's lattice dynamics model using vibrational density of states for constructing thermodynamic databases. Phys Chem Minerals 40:207–227

Jahn S, Rahner R, Dachs E, Mrosjo M, Koch-Müller M (2013) Thermodynamic properties of anhydrous and hydrous, β-Mg2SiO4. High Press Res Int J. doi:10.1080/08957959.2013.806498

Ji S, Wang Z (1999) Elastic properties of forsterite-enstatite composites up to 3 GPa. J of Geodynamics 28:147–174

Kajiyoshi K (1986) High-temperature equation of state for mantle minerals and their anharmonic properties, MS Thesis, Okayama University, Okayama, Japan

Kanzaki M (1987) Ultrahigh-pressure phase relations in the system Mg4Si4O12–Mg3Al2Si3O12. Phys Earth Plan Int 49:168–175

Kanzaki M (1991) Ortho/clinoenstatite transition. Phys Chem Minerals 17:726–730

Katsura T, Ito E (1989) The system Mg2SiO4-Fe2SiO4 at high pressures and temperatures: precise determination of stabilities of olivine, modified spinel, and spinel. J Geophys Res B 94:15663–15670

Katsura T, Yokoshi S, Song M, Kawabe K (2004) Thermal expansion of Mg2SiO4 ringwoodite at high pressures. J Geophys Res 109(B12209):1–10

Katsura T, Yokoshi S, Kawabe K, Shatskiy A, Geeth MA, Manthilake M, Zhai S, Fukui H, Chamathni HA, Hegoda I, Yoshino T, Yamazaki D, Matsuzaki T, Yoneda A, Ito E, Sugita M, Tomioka N, Hagiya K, Nozawa A, Funakoshi K-I (2009a) P–V–T relations of MgSiO3 perovskite determined by in situ X-ray diffraction using a large-volume high-pressure apparatus. Geophys Res Lett 36(L01305):1–6

Katsura T, Yokoshi S, Kawabe K, Shatskiy A, Geeth MA, Manthilake M, Zhai S, Fukui H, Chamathni HA, Hegoda I, Yoshino T, Yamazaki D, Matsuzaki T, Yoneda A, Ito E, Sugita M, Tomioka N, Hagiya K, Nozawa A, Funakoshi K-I (2009b) Correction to "P–V–T relations of MgSiO3 perovskite determined by in situ X-ray diffraction using a large-volume high-pressure apparatus". Geophys Res Lett 36(L16309):1–2

Kieffer SW (1979) Thermodynamics and lattice vibrations of minerals: 3 lattice dynamics and an approximation for minerals with application to simple substances and framework silicates. Rev Geophys Space Phys 17:35–59

Kojitani H, Oohata M, Inoue T, Akaogi M (2012) Redetermination of high-temperature heat capacity of Mg2SiO4 ringwoodite: measurement and lattice vibrational model calculation. Am Mineral 97:1314–1319

Kono Y, Irifune T, Higo Y, Inoue T, Barnhoorn A (2010) P–V–T relation of MgO derived by simultaneous elastic wave velocity and

in situ X-ray measurements: a new pressure scale for the mantle transition region. Phys Earth Plan Int 183:196–211

Krupka KM, Robie RA, Kerrick DM, Ito J (1985) Low-temperature heat capacities and derived thermodynamic properties of anthophyllite, diopside, enstatite, bronzite, and wollastonite. Am Mineral 70:249–260

Kung J, Li B, Uchida T, Wang Y, Neuville D, Liebermann RC (2004) In situ measurements of sound velocities and densities across the orthopyroxene → high-pressure clinopyroxene transition in MgSiO3 at high pressure. Phys Earth Planet Int 147:27–44

Kung J, Li B, Uchida T, Wang Y (2005) In-situ elasticity measurement for the unquenchable high-pressure clinopyroxene phase: implication for the upper mantle. Geophys Res Lett 32(L01307):1–4

Landau LD, Lifshitz EM (1980) Statistical Physics, 3, part 1 edn. Pergamon Press, Oxford

Li B, Woody K, Kung J (2006) Elasticity of MgO to 11 GPa with an independent absolute pressure scale: implications for pressure calibration. J Geophys Res B 111:11206

Li L, Wentzcovitch RM, Weidner DJ, Da Silva CRS (2007) Vibrational and thermodynamic properties of forsterite at mantle conditions. J Geophys Res B112:05206

Liu J, Zhang J, Flesch L, Li B, Weidner DJ, Liebermann RC (1999) thermal equation of state of stishovite. Phys Earth Planet Int 112:257–266

Matsui M, Parker SC, Leslie M (2000) MD simulation of the equation of state of MgO: application as a pressure calibration standard at high temperature and high pressure. Am Mineral 85:312–316

Morishima H, Kato T, Suto M, Ohtani E, Urakawa S, Utsumi W, Shimomura T, Kikegawa T (1994) The phase boundary between α- and β-Mg2SiO4 determined by in situ X-ray observation. Science 265:1202–1203

Navrotsky A (1995) Thermodynamic properties of minerals. In: Mineral physics and crystallography. A handbook of physical constants, AGU Reference Shelf 2

Navrotsky A, Pintchovski FS, Akimoto S-I (1979) Calorimetric study of the stability of high pressure phases in the systems CoO–SiO2 and "FeO"–SiO2, and calculation of phase diagrams in MO–SiO2 systems. Phys Earth Planet Int 19:275–292

Nishihara Y, Nakayama K, Takahashi E, Iguchi T, Funakoshi K-I (2005) P–V–T equation of state of stishovite to the mantle transition zone conditions. Phys Chem Minerals 31:660–670

Oganov AR, Dorogokupets P (2004) Intrinsic anharmonicity in equations of state and thermodynamics of solids. J Phys: Condens Matter 16:1351–1360

Oganov AR, Gillan MJ, Price GD (2005) Structural stability of silica at high pressures and temperatures. Phys Rev B 71(064104):1–8

Ono S, Katsura T, Ito E, Kanzaki M, Yoneda A, Walter MJ, Urakawa S, Utsumi W, Funakoshi K (2001) In situ observation of ilmenite-perovskite phase transition in MgSiO3 using synchrotron radiation. Geophys Res Lett 28:835–838

Othani E, Kumazawa M (1981) Melting of forsterite Mg2SiO4 up to 15 GPa. Phys Earth Plan Int 27:32–38

Pacalo REG, Gasparik T (1990) Reversals of the orthoenstatite-clinoenstatite transition at high pressures and high temperatures. J Geophys Res 95:15853–15858

Presnall DC, Gasparik T (1990) Melting of enstatite (MgSiO3) from 10 to 16.5 GPa and the forsterite (Mg2SiO4)-majorite (MgSiO3) eutectic ate 16.5 GPa: implications for the origin of the mantle. J Geophys Res B 95:15771–15777

Putnis A (1992) Introduction to mineral sciences. Cambridge University Press, Cambridge

Reynard B, Rubie DC (1996) High-pressure, high-temperature Raman spectroscopy study of ilmenite-type MgSiO3. Am Mineral 81:1092–1096

Robie RA, Hemingway BS (1995) Thermodynamic properties of minerals and related substances a 298.15 K and 1 bar (10^5 Pascals) pressure and at higher temperatures. United States geological survey bulletin NO. 2131

Ross NL, Shu J-F, Hazen RM (1990) High-pressure crystal chemistry of stishovite. Am Mineral 75:739–747

Sawamoto H (1987) Phase diagrams of MgSiO$_3$ at pressures up to 24 GPa and temperatures up to 2200 C: phase stability and properties of tetragonal garnet. In: Manghnani MH, Syono Y (eds) High pressure research in mineral physics. Terra Scientific, Tokyo, pp 209–219

Saxena SK (1996) Earth mineralogical model: gibbs free energy minimization computation in the system MgO–FeO–SiO$_2$. Geochim Cosmochim Acta 60:2379–2395

Shim S, Duffy TS, Shen G (2001) The post-spinel transformation in Mg$_2$SiO$_4$ and its relation to the 660-km seismic discontinuity. Nature 411:571–574

Speziale S, Zha C-S, Duffy TS (2001) Quasi-hydrostatic compression of magnesium oxide to 52 GPa: implications for the pressure–volume–temperature equation of state. J Geophys Res B 106:515–528

Stixrude L, Lithgow-Bertelloni C (2005) Thermodynamics of mantle minerals—I. Physical properties. Geophys J Int 162:610–632

Stixrude L, Lithgow-Bertelloni C (2011) Thermodynamic of mantle minerals—II. Phase equilibria. Geophys J Int 184:1180–1213

Suzuki I, Anderson OL (1983) Elasticity and thermal expansion of a natural garnet up to 1000 K. J Phys Earth 31:125–138

Suzuki A, Ohtani E, Morishima H, Kubo T, Kanbe Y, Kondo T, Okada T, Terasaki H, Kato T, Kikegawa T (2000) In situ determination of the boundary between wadsleyite and ringwoodite in Mg$_2$SiO$_4$. Geophys Res Lett 27:803–806

Svendsen B, Ahrens TJ (1987) Shock-induced temperatures of MgO. J J R Astr Soc 91:667–691

Tsuchiya J, Tsuchiya T, Wentzcovitch RM (2005) Vibrational and thermodynamic properties of MgSiO$_3$ postperovskite. J Geophys Res B 110:02204

Umemoto K, Wentzcovitch RM (2011) Two-stage dissociation in MgSiO$_3$ post-perovskite. Earth Planet Sci Lett 311:225–229

Vassiliou MS, Ahrens TJ (1981) Hugoniot equation of state of periclase to 200 GPa. Geophys Res Lett 8:729–732

Vinet P, Ferrante J, Rose JH, Smith JR (1989) Universal features of the equation of state of solids. J Phys: Condens Matter 1:1941–1963

Watanabe H (1982) Thermochemical properties of synthetic high-pressure compounds relevant to the Earth's mantle. In: Manghnani MH, Akimoto S (eds) High-pressure research in geophysics. Center for Academic Publications, Japan/Tokyo, Reidel/Dordrecht, pp 441–464

Wu Z, Wentzcovitch RM (2007) Vibrational and thermodynamic properties of wadsleyite: a density functional study. J Geophys Res 112(B12202):1–11

Wu Z, Wentzcovitch RM, Umemoto K, Li B, Hirose K, Zheng J-C (2008) Pressure-volume-temperature relations in MgO: an ultra-high pressure–temperature scale for planetary sciences applications. J Geophys Res 113:B06204

Yong W, Dachs E, Benisek A, Secco RA (2012) Heat capacity, entropy and phase equilibria of stishovite. Phys Chem Minerals 39:153–162

Yu YG, Wentzcovitch RM (2006) Density functional study of vibrational and thermodynamic properties of ringwoodite. J Geophys Res 111(B12202):1–8

Yu YG, Wentzcovitch Vinograd VL, Angel RJ (2011) Thermodynamic properties of MgSiO$_3$ majorite and phase transitions near 660 km depth in MgSiO$_3$ and Mg$_2$SiO$_4$: a first principles study. J Geophys Res 116(B02208):1–19

Yusa H, Akaogi M, Ito E (1993) Calorimetric study of MgSiO$_3$ garnet and pyroxene: heat capacities, transition enthalpies, and equilibrium phase relations in MgSiO$_3$ at high pressures and temperatures. J Geophys Res 98:6453–6460